PHAGE DISPLAY PEPTIDES FOR BREAST CANCER TARGETING

A Thesis presented to the Faculty of the Graduate School at

the University of Missouri-Columbia

In Partial Fulfillment

Of the Requirements for the Degree

Master of Science

---

by

MAURA K. BATES

Dr. Susan L. Deutscher, Thesis supervisor

December 2010

The undersigned, appointed by the Dean of the Graduate School,
have examined thesis entitled

PHAGE DISPLAY PEPTIDES FOR BREAST CANCER TARGETING

Presented by Maura K. Bates

A candidate for the degree of Master of Science

And hereby certify that in their opinion it is worthy of acceptance.

_____

Professor Susan L. Deutscher

_____

Professor Thomas P. Quinn

_____

Professor Silvia Jurisson

ACKNOWLEDGEMENTS

I would like to thank my advisor Susan L. Deutscher for her guidance and encouragement during my graduate studies. This work would not have been possible without her assistance and support. I would also like to thank my other advisors, Thomas P. Quinn and Silvia S Jurisson for their help and support during this project. I give thanks to Marie T. Dickerson and Jessica R. Newton for all the laboratory assistance, explanations, and encouragement during my graduate work. It would not have been the same experience without my lab family. I also acknowledge Terry Carmack, Lisa Watkinson, Said Figueroa, and Fabio Gallazzi for their support.

I would also like to thank Sara Drenkhahn, Victoria Hodgekinson, and Mette Søndergaard along with my fellow graduate students for their friendship and support during graduate school. To my friends both near and far, thanks for all the calls and cards full of encouragement. Most of all, thanks to my parents for instilling both a love of learning and a dedication to striving towards goals that have allowed me to complete this degree. I could not have done this without your love and support.

TABLE OF CONTENTS

ACKNOWLEDGEMENTS……..…...ii

LIST OF ILLUSTRATIONS……..iv

LIST OF TABLES……..….v

LIST OF ABBREVIATIONS…….....vi

ABSTRACT……..……...viii

Chapters

1. INTRODUCTION……..…….……1

2. ErbB-2 PEPTIDE RADIOIMAGING OF BREAST CANCER……..…...……10

Introduction
Materials and Methods
Results
Discussion
Conclusion

3. GALECTIN-3 PEPTIDE CHARACTERIZATION…….34

Introduction
Materials and Methods
Results
Discussion
Conclusion

4. SUMMARY……...53

REFERENCES……...…...54

LIST OF FIGURES

Figure Page Number

1- The chemical structure of DAP-GSG-KCCYLS and (NαHis)Ac-GSG-KCCYSL……...…28

2- RP-HPLC elution profile of DAP-GSG-KCCYSL and (NαHis)Ac-GSG-KCCYSL peptides with and without $^{99m}Tc(CO)_3$ radiolabeling...……..29

3- In *vitro* ErbB-2 receptor binding of $^{99m}Tc(CO)_3$-(NαHis)Ac-GSG-KCCYSL and $^{99m}Tc(CO)_3$-DAP-GSG-KCCYSL peptides……...30

4- In *vitro* blocking studies with $^{99m}Tc(CO)_3$-DAP-GSG-KCCYSL and $^{99m}Tc(CO)_3$-(NαHis)Ac -GSG-KCCYSL……..31

5- Tumor imaging with $^{99m}Tc(CO)_3$-DAP-GSG-KCCYSL peptide with and without the presence of the cold competitor Re-DAP- GSG-KCCYSL……...…32

6- Tumor imaging with $^{99m}Tc(CO)_3$-(NαHis)Ac -GSG-KCCYSL peptide with and without the presence of the cold competitor Re-(NαHis)Ac - GSG-KCCYSL……...…33

7- Binding of peptides to gal-3 displayed on cultured human tissue cells, MDA-MB-435 human breast cancer cells and PC-3 prostate cancer cells…...….49

8- Gal-3 peptides binding to immobilized gal-3 using ELISA experiments……..…50

9- Binding of biotinylated point mutation peptides to gal-3 displayed on cultured human tissue cells…….……...51

10- Intensity of binding of biotinylated point mutation peptides to gal-3 displayed on cultured human tissue cells……...52

LIST OF TABLES

Tables Page Number

1- Biodistribution of $^{99m}Tc(CO)_3$-DAP-GSG-KCCYSL and $^{99m}Tc(CO)_3$-(NαHis)Ac-GSG-KCCYSL in female SCID mice bearing MDA-MB-435 human breast carcinoma tumors……..27

2- Galectin-3 selected peptide G3C12 and Ala point mutation peptides and scrambled control peptide……..48

LIST OF ABBREVIATIONS

Abs, antibodies

Akt, phosphatidylinositol 3-kinase

BBN, Bombesin

BSA, bovine serum albumin

Cp, coat protein

Cpm, counts per minute

CT, Computerized axial tomography

DAP, diaminoproprionic acid

DIEA, N,N-Diisopropylethylamine

DOTA, 1,4,7,10-tetra-azacyclododecane- N,N',N''N'''-tetraacetic acid

ECD, extracellular domain

EGRF, epidermal growth factor receptor

ELISA, enzyme-linked immunosorbent assay

ErbB-2, Human epidermal growth factor receptor 2

Fab, antibody fragments

FBS, fetal bovine serum

G3-C12, peptide with sequence ANTPCGPYTHDCPVKR

gal-3, galectin-3

GI, gastrointestinal

HPLC, high performance liquid chromatography

HRP, horseradish peroxidase

IPTG, Isopropyl-ß-D-thiogalactopyranoside

LB, lysogeny broth also know as Luria broth

LC-MS, liquid chromatography- mass spectrometry

MAb, monoclonal antibody

MAPK, mitogen-activated protein kinase (mitogen)

NαHis, retroN alpha-carboxymethyl histidine

PBS, phosphate buffered saline

PET, positron emission tomography

PMSF, Phenylmethanesulfonylfluoride

rpm, revolutions per minute

SCID, severe combined immune deficiency

SPECT, single photon emission computed tomography

TBST, Tris-buffered saline tween 20

TEAP, triethylammonium phosphate

TF, Thomsen-Friedenreich

TLC, thin layer chromatography

PHAGE DISPLAY PEPTIDES FOR BREAST CANCER TARGETING

Maura Bates
Dr. Susan Deutscher, Dissertation Supervisor

Cancer cell surfaces differ from healthy cell surfaces allowing the detection of cancer targets on the cell. Use of these targets combined with radiolabeled targeting vehicles results in sensitive imaging agents. Peptide targeting vehicles have shown advantages over antibodies with rapid blood clearance and increased diffusion.

Human epidermal growth factor receptor 2 (ErbB-2) and galectin-3 (gal-3) are two targets for peptides, which have been shown to be over-expressed in a variety of tumors, including breast adenocarcinomas. ErbB-2 is involved in signal transduction pathways for cell growth and differentiation. Gal-3 is a lectin involved in carbohydrate-mediated cancer cell adhesion via contact with the tumor-specific Thomsen-Friedenreich (TF) disaccharide antigen, which increases metastasis from primary tumors.

Bacteriophage (phage) display is a technique using phage to select peptide sequences that bind to specific targets, such as ErbB-2 and gal-3. The target ErbB-2 was used to identify peptide KCCYSL, which was previously characterized and radiolabeled with ^{111}In. In this study, KCCYSL was radiolabeled by two different chelation chemistry methods and ^{99m}Tc to create two potential imaging agents. These radiolabeled peptides were analyzed both *in vitro* with breast cancer cell lines, and also *in vivo* performing biodistribution and breast tumor imaging studies in mouse models of breast cancer. Another target, gal-3, was used to identify peptide ANTPCGPYTHDCPVKR also using the phage display technique. In this study, to characterize the peptide and identify key residues for peptide interaction, *in vitro* cell binding and enzyme-linked immunosorbent assay experiments were done with various alanine point mutation peptides.

CHAPTER 1- INTRODUCTION

Breast cancer is the second most frequently diagnosed cancer in women in the United States with 254,000 new cases and 40,000 deaths per year [1]. At present, over 12% of all women will develop breast cancer (approximately 1 in 8) and of these women at least 25% will die from this disease because their cancer was not detected at a curable stage. One of the major reasons for the high 25% mortality rate is the inability to image and diagnose the small primary cancers before they metastasize [2]. Currently available screening tools such as mammography and breast examination miss up to 40% of early breast cancers and are less effective for young women who often have dense breast tissue and more aggressive tumor growth. Knowing this, the identification of biomarker targets that can be effectively imaged, facilitating early diagnosis with multiple treatment options is a priority [3].

Biomarkers are biological molecules found in blood, body fluids, and tissues that signal a normal or abnormal process, condition, or disease. They can be detected and measured quantitatively to indicate either healthy or diseased states. There have been several biomarkers that have been discovered in cancerous tissue, often found to be in much higher concentration than in healthy normal tissue. Two examples of these biomarkers are human epidermal growth factor receptor (EGFR) 2 and galectin-3 (gal-3).

One biomarker of importance is human EGFR 2 commonly known as ErbB-2. ErbB-2 is a large (185 kDa) protein that spans the cell membrane and is a member of the EGRF gene family of receptor tyrosine kinases [4]. This receptor is known to dimerize with other family members to activate several signaling pathways. Blocking these

pathways has been shown to result in increased cell death and decreased tumor growth [5].

ErbB-2 is often overexpressed in breast, ovary, lung and other cancers [5-8]. This receptor is overexpressed in ~20-30% of breast cancers and its overexpression or mutation in women correlates with aggressiveness, lower survival rates, resistance to tamoxifen, and shorter time to relapse [9]. ErbB-2 receptors are frequently overexpressed on breast cancer cells in comparison to normal breast tissue cells, and upon activation the receptor clusters to specific locations on cancer cells making this receptor a good biomarker and anti-cancer target [10-11]. In addition to breast tumors, ErbB-2 has been discovered in 21% of ovarian cancer tumors [12-13]. This is a good biomarker to target because there are many hundred thousand ErbB-2 receptors expressed on breast cancer cells.

Another biomarker for cancer diagnosis and therapy is galectin-3 (gal-3), one of the most essential lectins involved in cancer cell adhesion. Gal-3 is a member of the galectin family of soluble mammalian lectins recognizing terminal β-galactose residues [14]. While other targets are being explored for the development of cancer imaging agents, carbohydrate-lectin complexes as tumor targets have been relatively unexplored.

Gal-3 is expressed in several types of cancer including breast cancer and its expression correlates with tumor cell conversion to metastatic phenotype *in vivo* [15-16]. The major tumor-associated ligand for gal-3 is the Thomsen-Friedenreich antigen (TF), a galactose β1-3 N-acetylgalactosamine (Galβ1-3GalNAc) disaccharide expressed on up to 90% of human carcinomas including those of the breast [17-18]. It has been previously shown that TF promotes the expression of gal-3 in normal endothelial cells and various

cancer cells including those of the breast and prostate [19]. The TF antigen binding part is the terminal Galβ1-3GalNAc carbohydrate moiety, which is exposed on proteins and lipids in cancer cells and is masked by a sialic acid in normal cells [17]. Upon contact with TF on the surface of tumor cells, endothelial gal-3 rapidly redistributes to interact with the tumor and endothelial cells [18-21]. Thus, the concentration of gal-3 at sites of tumor cell interaction may provide an innovative approach to the imaging of TF-gal-3-expressing breast tumors and the early diagnosis of breast cancer.

Bacteriophage (phage) display is a technique that has been used to find targets for the biomarkers ErbB-2 and gal-3, and these targets can then be used as imaging agents for breast cancer cells. Normal development of cancer imaging or therapeutic compounds for clinical use has historically relied on natural products, screening compound databases, or engineered antibodies and structure-based drug design which can take years to find targets to desired biomarkers. Conversely, phage display utilizes phage, viruses that infect bacteria using host machinery to replicate, to identify compounds that interact with the desired biomarkers. Smith and coworkers utilized one class of phage called Fd to develop a high output combinatorial system that is now called phage display [22]. Phage particles (virions) themselves contain very small and easily manipulated genomes, and phage display utilizes this by fusing the native coat protein (cp) with different new sequences. Either the minor coat protein cpIII or the major coat protein cpVIII are used for this fusion [23]. Once this genetic fusion of the N terminus of the cp sequence to foreign peptide sequence occurs, the new "mutant" phage then expresses the new sequence as a peptide displayed on the surface of the virion. This peptide on the

virion surface allows for the selection of sequences that bind to a selected biomarker, such as ErbB-2 and gal-3.

Each phage encodes one peptide sequence and displays one peptide sequence, though there can be many copies, but a library can be composed of many different phages with different displayed peptides. Instead of finding genetically engineered peptides or proteins one by one, it is easier to generate large populations of phages displaying millions of different inserted sequences to form random peptide libraries to be used in phage display libraries. The most commonly used libraries today are based on the fUSE5 vector, which contains five copies of a fifteen amino acid fused peptide within the N-terminus of cpIII after the Ala at residue 8, and the f88-4 vector, which contains up to 100 copies of the fifteen amino acid foreign peptide displayed on the N-terminus of cpVIII also after the Ala at residue 8. The resulting amplification of interacting molecules in subsequent rounds of "affinity selection", a process of round of selection, elution, and amplification, can yield very rare, specific binders from an enormous collection of molecules. After selection, the amino acid sequence corresponding to the displayed peptide is deduced by DNA sequencing of the foreign insert.

Phage display can be used to identify antibodies (Abs), antibody fragments (Fab), and peptide sequences that interact with biomarkers such as ErbB-2 and gal-3. Antibodies are the most common biological targeting vehicles for the specific delivery of a radionuclide to a tumor [24-26]. Whole Abs are large (~140kDa), which results in long biodistribution times *in vivo*, slow tumor penetration and slow clearance rates through the hepatobiliary system that can damage the liver which limit their usefulness for imaging and therapy [27]. To avoid these problems, Fab of smaller sizes have been produced,

which result in Fab clearance though the kidneys but often lower target affinities which reduce effectiveness. While there are some tumor associated antigens and antibodies being explored in drug discovery, there is a vital need to explore new targets and develop new targeting vehicles. Peptides have been shown to offer advantages over Abs and Fab for *in vivo* because of their rapid blood clearance, increased diffusion, non-immunogenic use, and ease of synthesis [28-31] .

Many targeting vehicles have been used for ErbB-2, including monoclonal antibodies [32], immunoconjugates [33], vaccines [34], antisense therapy and gene therapy [35]. Herceptin (Trastuzumab; Genentech, San Francisco, CA) a humanized monoclonal antibody against ErbB-2 has been the first to reach widespread clinical use for the treatment of metastatic breast cancer [36-37]. Unfortunately, the drug Herceptin was found to decrease the function of doxorubicin, another commonly used cancer drug, and may damage heart muscle tissue on its own [36-37]. In previous studies [38], peptides were identified from a phage display library using affinity selection against recombinant extracellular domain of human ErbB-2 (ErbB-2-ECD), and one peptide KCCYSL represented 75% of the selected population. The KCCYSL peptide showed recognition of the recombinant ErbB-2-ECD with Enzyme-linked immunosorbent assay (ELISA) where bound Erb-2-ECD interacts with soluble biotinylated peptide, which is then calorimetrically developed. Also the KCCYSL peptide showed recognition of human breast and prostate cancer cells overexpressing ErbB-2 with cell binding experiments where biotinylated peptide bound to cells was analyzed by fluorescent microscopy [38] . In other previous studies [39], the specificity, affinity, and key binding residues of the

KCCYLS peptide were investigated. Compiling all of these results, the peptide KCCYLS is a good target peptide to use for investigation with the biomarker ErbB-2.

While there has been little application of carbohydrate-lectin interactions for use as imaging agents, there has been preliminary work in that direction. Peptides have been found that target the TF antigen [19, 40-42], and gal-3 [43-44] In a previous study, peptide ANTPCGPYTHDCPVKR called G3-C12 was found to bind to purified gal-3 and preferentially to cultured carcinoma cells known to express gal-3 over cells not expressing gal-3 [44]. Further study on the key residues of this sequence occurred, with plans to use peptide G3-C12 as a target peptide for use in gal-3 containing tumor imaging.

Attachment of radiometals to the peptides KCCYSL and G3-C12 would allow for radioimaging of the cells with the ErbB-2 and gal-3 biomarkers. There have been relatively few identified tumor-targeting radiolabeled peptides that can be used as imaging agents *in vivo*, but this area has great potential for tumor imaging agents [45]. One of the possible reasons for poor *in vivo* results may include the hydrophobic nature of peptides selected and poor peptide radiometal combination. Once peptides are selected using phage display technique, study of the potential for imaging agents occurs, beginning with the choice of radiometal.

There are several common radiometals used for radiolabeling, including technetium 99m (^{99m}Tc), indium 111 (^{111}In), and copper 64 (^{64}Cu). One widely used radioisotope for diagnostic imaging is ^{111}In, which has a 2.8 day half-life with 173 and 247 keV gamma emissions [46]. ^{111}In-labeled peptide pentetreotide (Octreoscan™) is in clinical use for imaging somatostatin receptor positive tumors [47-48], while ^{111}In-labeled platelets and white blood cells have been used to image thrombi and sites of

infection and inflammation [49], showing the potential for ^{111}In labeled diagnostic peptides. This radiometal was previously used for labeling KCCYSL and has shown potential for use as an imaging agent [38]. However, ^{111}In is typically produced offsite and shipped to labs for drug trials, allowing for radioactive decay before its use. An improvement might occur with use of another commonly used radioisotope, ^{99m}Tc [50-51]. ^{99m}Tc is one of the most widely used diagnostic radionuclides because of its short half life (6 h) and low energy emissions (140 keV gamma emission). Production from a ^{99}Mo/^{99m}Tc generator system, which is commonly onsite in hospitals and research labs, results in a radionuclide with less shipment time and subsequent decay of radioactive material. Radioimaging based on ^{99m}Tc has been used for myocardial function, cerebral blood flow, renal function and numerous other conditions. [51]. The development of tumor targeting radiopharmaceuticals based on ^{99m}Tc have generally involved Tc(V) oxo and Tc(I)-tricarbonyl cores because of the ease of reduction to Tc(V) from pertechnetate with common kits and the availability of ^{99m}Tc precursors $^{99m}Tc(CO)_3(OH_2)^+$ [52].

The selection of radiometals is made based on the instrument to be used for the imaging. Two common techniques are Single Photon Emission Computed Tomography or SPECT and Positron Emission Tomography or PET. Both techniques require an injection of radiolabeled substance into the body. SPECT scans are done using radionuclides that emit gamma photons such as ^{99m}Tc and ^{111}In. A SPECT camera measures the emitted gamma photons directly as they leave the body, and then a computer compiles together all the emissions to create a 3D image of where the radiolabeled substance is localized, ie the tumor. A PET scan uses radionuclides that emit positron emissions, such as ones from ^{18}F and ^{64}Cu. PET scans differ in that the

positrons that are emitted from the radio nuclide are not measured directly but rather interact with nearby electrons, which then annihilate and emit two photons in opposite directions. The camera detects these two photons from one single positron emission, which provide more information to determine precise localization of the radiolabeled substance. This results in PET having the advantages of more sensitivity by 1-2 orders of magnitude and quantitative measurements over SPECT. However, the lower cost and availability of SPECT machines results in 10 times as many SPECT scans as PET scans available in hospitals [53]. This project focuses on ^{99m}Tc labeled peptides for SPECT, but similar techniques could be used to attach other radiometals such as ^{64}Cu for PET scans.

Once the biomarker targeting peptide and appropriate radiometal have been identified, the components of an imaging agent can be assembled. Our previous work includes extensive experience imaging with ^{99m}Tc- and ^{111}In- labeled peptides [39, 43, 54-58]. For the biomarker ErbB-2, the targeting peptide KCCYSL will be used with ^{99m}Tc for production of a SPECT imaging agent. The radiometal can be directly attached to the target peptide, or attached with a chelator linker molecule between the radiometal and the target peptide. It has been shown that direct attachment of the radiometal to its target can result in the disruption of disulfide bridges within the target molecule [59]. Therefore, since the target peptide has an amino acid group, which potentially forms disulfide bridges, it would be beneficial to use a chelator group to protect the target sequence. First, the peptide is created with a Gly- Ser- Gly (GSG) amino acid linker attached to the NH_2 terminus of the peptide, which reduces the steric hindrance between the peptide and chelator and also allows the direction of the radiometal attachment to the NH_2 terminus of

the peptide. The chelator is attached to the linker, and also provides the interaction between the radiometal and the peptide complex. Previous studies have used the chelator 1,4,7,10-tetraazacyclododecane- N,N',N''N'''-tetraacetic acid (DOTA) with ^{111}In, but new chelators will be used because DOTA does not work well for ^{99m}Tc chelation as shown by a lack of publications utilizing ^{99m}Tc DOTA chelation. The two chelators that will be included in this study are the ^{99m}Tc-carbonyl chelators diaminoproprionic acid (DAP) and retroN$^{\alpha}$-carboxymethyl histidine (Nα His) [60-62]. Employing two chelation strategies allows an evaluation of the two strategies and which yields the higher tumor to background distribution *in vivo* should translate into the best imaging agent for animal studies.

The purpose of this study is to take novel biomarker targeting peptides and develop them into diagnostic cancer imaging agents. Preliminary data for the G3-C12 peptide indicates that this peptide could be used with proper chelators and radiometals to produce an imaging agent. However, before *in vivo* tests of G3-C12 peptide imaging agents can begin, a better understanding of the interaction of the peptide sequence with bound compounds such as gal-3 must occur. Another biomarker, ErbB-2, and target peptide, KCCYLS, pair has been previously developed into an imaging agent. ^{99m}Tc-labeled KCCYSL is being developed and has more immediate translatability to clinical application than previously investigated ^{111}In KCCYSL because of better accessibility of hospitals to ^{99m}Tc generators. The improvement of hospital ready imaging agents in combination with SPECT imaging can be used for the early diagnosis of cancer patients in the earlier stages of cancer; ultimately lowering the mortality rate for breast cancer patients, with enhanced treatment efficiencies.

CHAPTER 2- ErbB-2 PEPTIDE RADIOIMAGING OF BREAST CANCER

INTRODUCTION

^{99m}Tc is a nearly ideal radionuclide for Single Photon Computed Emission Tomography (SPECT) imaging in nuclear medicine due to its favorable decay properties [$t_{1/2}$=6.04 h, Eγ=140kev (89%)] and its economical production from ^{99}Mo/^{99m}Tc generator systems [52]. The chemistry for labeling peptides and proteins with ^{99m}Tc directly or via bifunctional chelators is well established [52]. Advances in the development of organometallic compounds and their cognate chelators for labeling biomolecules with ^{99m}Tc has lead to an explosion of radiopharmaceutical molecules labeled with low oxidation state +1 ^{99m}Tc-tricarbonyl [^{99m}Tc(CO)$_3$] cores. The successful development of a kit preparation for the synthesis of the *fac*-[^{99m}Tc(OH$_2$)$_3$(CO)$_3$]$^+$ aquaion as a radiosynthon has lead to the development of ^{99m}Tc(CO)$_3$ labeled antibodies, peptides, sugars and nucleotides [63-64]. Because of the low–spin, d^6 electronic configuration of Tc (I), the ^{99m}Tc(CO)$_3$ core is remarkably stable over a wide range of pH values. By simply functionalizing the NH_2 terminus of Bombesin (BBN) analogues with diaminopropionc acid (DAP) or (Nα-histidinyl) acetic acid [(NαHis)Ac], the BBN analogues were successfully radiolabeled by [^{99m}Tc(OH$_2$)$_3$(CO)$_3$]$^+$ radiosynthon, obtaining high specific radioactive peptides. Moreover, biological activity of the peptide was maintained [65-67].

ErbB-2 is a member of the epidermal growth factor receptor (EGFR) family of transmembrane receptor tyrosine kinases, consisting of ErbB-1, ErbB-2, ErbB-3 and ErbB-4 [68]. While no known ligand or growth factor has been identified for ErbB-2, it heterodimerizes with other family members activating several signaling pathways

including mitogen-activated protein kinase (MAPK) and the phosphatidylinositol 3-kinase (Akt) pathways [6, 69-70]. An activated MAPK pathway results in increased cancer cell adhesion, growth, and angiogenesis, while an activated Akt pathway leads to upregulation of the Bcl-2 gene and cancer cell survival. ErbB-2 has received much attention both as a biomarker for breast and prostate cancer and as a target for specific cancer imaging and therapeutic agent development. ErbB-2 is overexpressed in ~20-30% of breast cancers and its overexpression or mutation in women correlates with tumor aggressiveness and high mortality rates [71]. Antibodies have been developed to target and/or block the action of ErbB-2 either by directly targeting ErbB-2 or its interacting partners and ligands. In particular, agents that block ErbB-2-mediated dimerization and/or receptor signaling are being explored for directed cancer imaging and therapy. A humanized murine monoclonal antibody (MAb), trastuzumab (Herceptin®; Genetech, Inc.) has been evaluated for the targeting of the ErbB-2 receptor on breast carcinomas [25, 72]. Trastuzumab was the first such agent to reach widespread clinical use for the treatment of metastatic breast cancer [25]. The anti-ErbB-2 MAb 2C4 is showing promise even in cancers where ErbB-2 receptor surface density is low [73]. Another antibody pertuzumab (Omnitarg; Genetech, Inc.) blocks ErbB-2-ErbB-1 heterodimerization, and has activity in non-ErbB-2 overexpressing tumors [74]. Results with ErbB-2-targeting antibodies have been mixed since many patients develop drug resistance and toxicity problems. Thus, new molecules and modalities are being developed to target ErbB-2, and include peptides, vaccines, antisense technology and gene therapy [69-70].

Peptides have been shown to exhibit less toxicity and possess better pharmacokinetic properties, such as higher target to background ratios and fast blood

clearance, compared to large antibodies and their fragments [31, 75-76]. In previous studies, the peptide, KCCYSL, was selected from a random bacteriophage (phage) peptide display library screened against the extracellular domain of ErbB-2 receptor [19]. KCCYSL exhibited limited homology with several proteins that potentially interact with the ErbB family of receptors [38]. Experimental results showed that KCCYSL was capable of specifically binding the ErbB-2 receptor with 295 nM affinity. Previously, the KCCYSL peptide was conjugated with DOTA via a Gly-Ser-Gly (GSG) spacer and radiolabeled with ^{111}In [39]. The ^{111}In-DOTA-GSG-KCCYSL peptide bound ErbB-2—expressing human breast carcinoma cells *in vitro*. Biodistribution patterns exhibited rapid tumor uptake and whole body clearance of ^{111}In-DOTA-GSG-KCCYSL in human breast carcinoma-bearing SCID mice, and SPECT/CT studies demonstrated that the breast tumor was readily visualized by the radiolabeled peptide conjugate at 2 h post injection. This finding suggested that the KCCYSL peptide has the potential to be used as a vehicle for the specific delivery of radionuclides or cytotoxic agents to cancer cells for diagnostic and therapeutic purposes.

In the present study the ErbB-2 targeting peptide KCCYSL, conjugated to DAP or (Nα-His)Ac via a GSG spacer, was radiolabeled with the $[^{99m}Tc(H_2O)_3(CO)_3]^+$ radiosynthon. The purified radiolabeled peptides were analyzed for binding to cultured MDA-MB-435 human breast carcinoma cells. Furthermore, the biodistribution properties and (SPECT) imaging of the two radiolabeled peptides were assessed in SCID (ICR SCID) female mice bearing human MDA-MB-435 breast tumors.

MATERIALS AND METHODS

2.1 Chemicals and Reagents

^{99m}Tc was purchased from Mid America Isotopes (Columbia, MO). All peptide synthesis reagents were purchased from Novabiochem (San Diego, CA) or Genzyme (Cambridge, MA). H-His(1Trt)-OtBu was purchased from Bachem Americas, Inc. (Torrance, CA). All other reagents were obtained from Fisher Scientific Co. (Pittsburg, PA) unless otherwise specified.

2.2 Cell Lines and Cell Culture

Human breast carcinoma cell line MDA-MB-435 and human leukemia cell line K562 were received from American Type Tissue Culture (Manassas, VA). The cells were maintained as monolayer cultures in RPMI 1640 Custom media (Invitrogen, St. Louis, MO) with 10% FBS and 0.06 mg/mL gentamycin. Cultures were maintained at 37°C in a 5% CO_2 humidified incubator.

2.3 Peptide Synthesis

Peptides were synthesized in a model 396 multiple peptide synthesizer (Advanced Chem Tech, Louisville, KY) using solid-phase Fmoc chemistry. Cleavage and side chain deprotection were achieved by treating the resin with 87.5% trifluoroacetic acid / 2.5% thioanisole / 2.5% phenol / 2.5% water / 2.5% ethandithiol / 2.5% triisopropylsilane. The peptides were purified by semipreparative High Performance Liquid Chromatography (HPLC) (Beckmann Coulter, Fullerton, CA). Crude and pure peptide preparations were characterized by Liquid Chromatography-Mass Spectrometry (LC-MS) (Thermo Finnigan, San Jose, CA).

2.4 Preparation of Nα-His-Ac-GSG-KCCYSL

The free amino H_2N-GSG-KCCYLS protected peptidyl-resin was treated with bromoacetyl bromide (20 eq) and N,N-diisopropylethylamine (DIEA) (5 eq) to obtain the reactive bromoacetylated intermediate (Br-CH_2CO-NH-GSG-KCCYLS protected peptidyl-resin).

Subsequently, nucleophilic substitution of the bromine with the amino group of H-His(1Trt)-OtBu (5 eq in presence of 5 eq of DIEA) resulted in the desired crude target molecule, which after cleavage from the resin and deprotection was analyzed by LC-MS and purified by preparative HPLC.

2.5 Peptide Radiolabeling

The ^{99m}Tc-labeling of DAP-GSG-KCCYSL and (NαHis)Ac-GSG-KCCYSL occurred in two steps. The first step utilized the Isolink™ kit (Mallinckrodt, St. Louis MO) to produce the intermediate synthon $[^{99m}Tc(CO)_3(OH_2)_3]^+$ according to the manufacturer's instructions. $^{99m}TcO_4^-$ (1.0 mL) from a commercial generator (20-100 mCi) was added to the IsoLink vial and incubated in a boiling water bath for 20 min. The $[^{99m}Tc(CO)_3(OH_2)_3]^+$ yield was determined by Thin Layer Chromatography (TLC), using a silica GF_{254} aluminum plate as stationary phase and CH_3OH:HCl (36%) =99:1 as mobile phase, with $^{99m}TcO_2$ (Rf = 0.0), $[^{99m}Tc(OH_2)_3(CO)_3]^+$ (Rf = 0.4-0.6), and $[^{99m}TcO_4]^-$ (Rf = 1.0). The $[^{99m}Tc(CO)_3(OH_2)_3]^+$ solution was neutralized with 0.1 N HCl to pH 7.4 immediately prior to use. DAP-GSG-KCCYSL or (NαHis)Ac-GSG-KCCYSL (100 µL of a 1mg/mL stock) was then added to 300 µL of the neutralized $[^{99m}Tc(CO)_3(OH_2)_3]^+$ and incubated at 75°C for 60 min. The peptide labeling yield was determined by TLC, using a silica GF_{254} aluminum plate as stationary phase and dextrose buffer (9.9g sodium citrate, 6.7g of dextrose in 1L of water) as mobile phase, with

$^{99m}Tc(CO)_3$-peptide (Rf = 0.0) and $[^{99m}Tc(OH_2)_3(CO)_3]^+$ (Rf = 1.0). The radiolabeled peptide conjugates were purified using HPLC with a C18 reversed-phase column. Solvent A was triethylammonium phosphate (TEAP) 0.05 M in water (pH 2.25) and solvent B was methanol (100%). A gradient with solvents A and B was run as follows: 0-5 min, 100% A; 5-6 min, 100-75% A; 6-9 min, 75-66% A; 9-25 min, 66-0% A; 25-29 min, 0% A; 29-34 min, 0-100% A; 34-38 min, 100% A. The radiolabeled peptides were concentrated on a C-18 Sep-pak cartridge, eluted with MeOH and dried under a stream of N_2 gas at 60˚C. The radiolabeled peptides were reconstituted in 0.9% saline. The radiochemical stability of $[^{99m}Tc(CO)_3]$-labeled peptides was analyzed by RP-HPLC after a 24 h incubation with pH 7.4 10 mM phosphate-buffered solution (PBS).

2.6 In Vitro Cell Binding

Experiments to test the ability of the radiolabeled peptides to bind to cells expressing ErbB-2 (human breast carcinoma MDA-MB-435 cells) or to cells that express very low levels of ErbB-2 (human leukemia K562 cells) were performed. Cells grown in flasks were released with cell dissociation buffer (Ca^{2+} and Mg^{2+} free phosphate based saline) and washed once with cell binding media (MEM with 25 mM HEPES, 0.02% BSA, 0.3 mM 1,10-phenanthroline) (Invitrogen, St. Louis, MO). Cells (1.25×10^6) were transferred to small microcentrifuge tubes containing 8×10^4 cpm of radiolabeled peptide for a total volume of 0.35 mL. After mixing, the samples were incubated at 37°C for different times (1 min, 30 min, 1 h, 2h, and 4 h). After incubation, the medium was removed by centrifugation and aspiration, and the cells were resuspended with ice-cold Dulbecco's PBS (Invitrogen, St. Louis MO). This process was repeated two more times. The final pellets were resuspended in PBS and transferred to a new microcentrifuge tube

prior to counting. Radioactivity bound to the cells was quantitated in a Wallac gamma counter (PerkinElmer Life and Analytic Science Inc., Waltham, MA) Cell binding ability was reported as total radioactivity in counts per minute (cpm) bound to the cells. The time course cell binding experiment also contained 2 hour time points in which 2 μg or 5 μg of $Re(CO)_3$-DAP-GSG-KCCYSL or $Re(CO)_3$-(NαHis)Ac-GSG-KCCYSL was added to the same amount of cells and peptide. After 2 hours of incubation, the blocked cells were treated as stated previously.

2.7 Animal Studies

All animal studies were conducted in compliance with Institutional Animal Care rules for the conduct of animal experimentation. Female 4-6 wk old SCID (ICR SCID) mice (Taconic, Hudson, NY) were inoculated subcutaneously in the shoulder with $5x10^6$ cultured MDA-MB-435 human breast carcinoma cells. The biodistribution and SPECT/CT imaging of the $[^{99m}Tc(CO)_3]$-radiolabeled peptides were examined in the MDA-MB-435 breast carcinoma bearing mice, when the tumors reached approximately 0.5g.

2.8 In Vivo Biodistribution Studies

The pharmacokinetics of the $[^{99m}Tc(CO)_3]^+$-radiolabeled peptides were determined in the SCID female mice bearing MDA-MB-435 human breast carcinoma tumors. Approximately 5-40 μCi of HPLC purified $[^{99m}Tc(CO)_3]^+$-radiolabeled peptides were injected into the mouse via the tail vein. Mice (n=4) were euthanized at 1, 2, 4, 24 h post injection, with tumors and organs of interest harvested, weighed and radioactivity quantitated in a gamma counter. Blood values were taken as 6.5% of the whole-body weight. Blocking studies to demonstrate selective binding of the purified $[^{99m}Tc(CO)_3]^+$-

labeled peptides were performed in SCID female mice bearing MDA-MB-435 human breast carcinoma tumors (n=3) by injection of the non-radiolabeled $[Re(CO)_3]$- peptide [21,22] followed by the corresponding $[^{99m}Tc(CO)_3]^+$-labeled peptide 15 min later. The blocking efficiency was evaluated 2 h post injection of the radiolabeled peptide. Uptake of radioactivity in the tumor and normal tissues and organs was expressed as a percentage of the injected radioactivity dose (%ID) per gram or as %ID of tissue. Statistical comparisons between groups were performed by the unpaired Students t test. A *p* value of 0.05 or less was considered statistically significant.

2.9 MicroSPECT/CT Imaging Studies

Imaging studies were performed by injecting 0.5 mCi of ^{99m}Tc-DAP-GSG-KCCYSL or ^{99m}Tc-(NαHis)Ac-GSG-KCCYSL into the tail vein of MDA-MB-435 tumor bearing mice. Blocking studies were performed by injecting 200 μg of the non-radiolabeled $[Re(CO)_3]$- peptide 15 min prior to injection of the corresponding radiolabeled peptide. At 2 h post injection, the mice were anesthetized with isoflurane and imaged with a microSPECT/CT system (Siemens Preclinical Solutions, Malvern, PA) equipped with high-resolution 2-mm pinhole collimators. SPECT and CT images were coregistered using Ascent Media System & Technology Service 3.1, (Northvale, NJ).

RESULTS

3.1 Radiolabeling

fac-$[^{99m}Tc(OH_2)_3(CO)_3]^+$ was prepared *via* an IsoLink™ kit per the manufacturer's instructions. The ^{99m}Tc-radiolabeling yield of the ErbB-2 receptor

targeting peptides DAP-GSG-KCCYSL and (NαHis)Ac-GSG-KCCYSL was ~70% (Figure 1). High specific activity peptides were obtained via RP-HPLC purification that was capable of separating the radiolabeled peptide from excess non-radiolabeled peptide and uncomplexed ^{99m}Tc. The retention times of $^{99m}TcO_4^-$, *fac*-$[^{99m}Tc(OH_2)_3(CO)_3]^+$, DAP/(NαHis)Ac-GSG-KCCYSL, and ^{99m}Tc-DAP/(NαHis)Ac-GSG-KCCYSL were 4.0 min, 8.0 min, 14.9 min, and 18.5 min, respectively. The purification resulted in single, high-concentration species as determined by analytical HPLC analysis (Figure 2). Both ^{99m}Tc-DAP-GSG-KCCYSL and ^{99m}Tc(NαHis)Ac-GSG-KCCYSL exhibited high stability after a 24 h incubation in 10 mM phosphate-buffered solution (pH 7.4), as determined by RP-HPLC. The radiochemical purity of both compounds was greater than 92% (data not shown).

3.2 In Vitro Cell Binding

The interaction of radiolabeled peptides with ErbB-2 expressing carcinoma cells was studied to determine if the peptides retained binding affinity for ErbB-2. *In vitro* experiments were performed with ^{99m}Tc-DAP-GSG-KCCYSL and ^{99m}Tc-(NαHis)Ac-GSG-KCCYSL peptides using MDA-MB-435 human breast carcinoma cells, which express moderate levels of ErbB-2, and K562 cells, which express very low levels of ErbB-2. The binding ability of the radiolabeled peptides to ErbB-2 was analyzed *in vitro* by incubating radiolabeled peptide conjugates with MDA-MB-435 or K562 cells for various times at 37º C. Binding of the peptides to the cells increased gradually, leveling off at 2 h. No significant increase in binding was observed after that time, indicating saturated binding of the peptide to the cells. A cell binding capacity of approximately 4% was obtained for ^{99m}Tc-(NαHis)Ac-GSG-KCCYSL peptide (Figure 3A) and 7% was

obtained for ^{99m}Tc-DAP-GSG-KCCYSL peptide (Figure 3B) with respect to the total radioactivity added to the cells.

The specific binding of ^{99m}Tc-DAP-GSG-KCCYSL and ^{99m}Tc-(NαHis)Ac-GSG-KCCYSL peptides was tested by addition of cold Re conjugated peptides. Re-DAP-GSG-KCCYSL or Re-(NαHis)Ac-GSG-KCCYSL blocking peptide was added to tubes containing the same amount of cells and ^{99m}Tc-radiolabeled peptide and incubated for 2 h. This study was done with both MDA-MB-435 cells and K562 cells, and with 2.7 E-13 M of radiolabeled peptide, calculated using activity. After subtraction of the nonspecific binding signal, it was found that using 1.04 E-7 μg of ^{99m}Tc-DAP-GSG-KCCYSL peptide, 2 μg of Re block (4.5 E-6 M) decreased the specific binding signal by 42% and 5 μg of Re block (1.1E-5 M) decreased the specific binding signal by 100%, effectively blocking the specific binding of the ^{99m}Tc-labeled peptide to the ErbB-2 receptor (Figure 4A). Using 1.14 E-7 μg of ^{99m}Tc- (NαHis)Ac-GSG-KCCYSL peptide, 2 μg of Re block (4.2 E-6 M) decreased the specific binding signal by 6% and 5 μg of Re block (1.0 E-5 M) decreased the specific binding signal by 51% (Figure 4B). The K_d for ^{111}In labeled DOTA-KCCYSL has been previously determined to be 295 ± 56 E-9 M; in comparison this experiment is using twenty and fifty fold greater amounts of blocking peptide [39].

3.3 In Vivo Biodistribution Studies

The biodistribution properties of the ^{99m}Tc-DAP-GSG-KCCYSL and ^{99m}Tc-NαHi-GSG-KCCYSL peptides were examined in female SCID mice bearing MDA-MB-435 human breast tumors. The tumor and organ distributions of the radiolabeled peptides at 1, 2, 4, and 24 h and the 2 h Re block are shown in Table 1. Tumor uptake of the ^{99m}Tc-DAP-GSG-KCCYSL was 1.67 ±0.16, 1.25 ±0.61, and 0.88 ±0.12 %ID/g at 1, 2,

and 4 h, respectively. Tumor uptake of the ^{99m}Tc-(NαHis)Ac-GSG-KCCYSL was 0.76 ±0.13, 0.75 ±0.40, and 0.33 ±0.08 %ID/g at 1, 2, and 4 h, respectively, indicating tumor retention of the peptide.

Whole-body disappearance of radioactivity was rapid, with 73% ID in the urine after 1 h and 81% ID after 4 h for ^{99m}Tc-DAP-GSG-KCCYSL, and 72% ID and 80% ID for ^{99m}Tc-(NαHis)Ac-GSG-KCCYSL, respectively. Radioactivity levels in the blood were 2.65 ±0.26 %ID/g at 1 h post injection followed by 1.65 ±0.34 %ID/g at 2 h and 1.29 ±0.34 %ID/g at 4 h for ^{99m}Tc$(CO)_3$-DAP-GSG-KCCYSL. Blood levels were 1.66 ±0.08 %ID/g at 1 h post injection followed by 1.30 ±0.65 %ID/g at 2 h and 1.05 ±0.15 %ID/g at 4 h for ^{99m}Tc$(CO)_3$-(NαHis)Ac-GSG-KCCYSL. Both peptides showed clearance from the blood by 2 h post injection of the peptides.

Normal organ uptake of radioactivity peaked in the kidneys, with uptake also in the intestines, lungs and liver. Radioactivity in the kidneys declined from a peak of 8.43 ±0.82 %ID/g at 1 h to 4.39 ±1.89 %ID/g at 4 h and 0.91 ±0.24%ID/g at the end of 24 h for ^{99m}Tc-DAP-GSG-KCCYSL and 9.93 ±0.75%ID/g, 4.37 ±0.59%ID/g, and 1.51 ±0.17%ID/g at 1, 4, and 24 h, respectively for ^{99m}Tc-(NαHis)Ac-GSG-KCCYSL.

Radioactivity in the liver declined from a peak of 3.92 ±0.26%ID/g, 1.84 ±0.52%ID/g, and 0.35 ±0.08%ID/g at 1, 4, and 24 h, respectively for ^{99m}Tc-DAP-GSG-KCCYSL and 2.01 ±0.08 %ID/g at 1 h to 1.53 ±0.22 %ID/g at 4 h and 0.75 ±0.09%ID/g at the end of 24 h for ^{99m}Tc-(NαHis)Ac-GSG-KCCYSL. Radioactivity in the intestines increased from 2.87 ±0.32%ID/g to 4.35 ±1.22%ID/g at 1 and 4 h, and reduced to 0.20 ±0.04%ID/g at 24 h for ^{99m}Tc-DAP-GSG-KCCYSL. Radioactivity in the intestines increased from 5.29 ±0.84 %ID/g at 1 h to 6.36 ±1.47 %ID/g at 4 h, and then dropped to

0.31 ±0.07%ID/g at the end of 24 h for ^{99m}Tc-(NαHis)Ac-GSG-KCCYSL. These results indicate that clearance of the radiolabeled peptide also occurred through the hepatic system. Radioactivity in the lungs declined from 4.35 ±0.29%ID/g, 2.19 ±0.33%ID/g, and 0.30 ±0.07%ID/g, at 1, 4, and 24 h, respectively for ^{99m}Tc-DAP-GSG-KCCYSL and 1.21 ±0.11 %ID/g at 1 h to 0.78 ±0.08 %ID/g at 4 h and 0.39 ±0.02%ID/g at the end of 24 h for ^{99m}Tc-(NαHis)Ac-GSG-KCCYSL. The tumor uptake was much higher than muscle uptake, with tumor to muscle ratios of 5.31, 6.95, and 5.70 for 1, 2 and 4 h with ^{99m}Tc-DAP-GSG-KCCYSL. Tumor to muscle ratios of 4.32, 6.92, and 3.39 at 1, 2 and 4 hours were obtained for ^{99m}Tc-(NαHis)Ac-GSG-KCCYSL.

The specificity of tumor uptake of the ^{99m}Tc-DAP-GSG-KCCYSL and ^{99m}Tc-(NαHis)Ac-GSG-KCCYSL peptides *in vivo* was further evaluated by performing competition experiments with Re labeled peptides. The results indicated that tumor uptake of the radiolabeled peptide was blocked by approximately 30% for ^{99m}Tc-DAP-GSG-KCCYSL and 21% for ^{99m}Tc-(NαHis)Ac-GSG-KCCYSL.

3.4 SPECT/CT Tumor Imaging

The tumor targeting efficacy of ^{99m}Tc(CO)$_3$-DAP-GSG-KCCYSL and ^{99m}Tc(CO)$_3$-(NαHis)Ac-GSG-KCCYSL in SCID female mice bearing MDA-MB-435 human breast carcinomas were evaluated by performing SPECT/CT imaging 2 h post peptide injection.

Images of ^{99m}Tc(CO)$_3$-DAP-GSG-KCCYSL (Figure 5A and B) and ^{99m}Tc(CO)$_3$-(NαHis)Ac-GSG-KCCYSL (Figure 6A and B) demonstrated that the human breast carcinoma tumor could be visualized at 2 h post injection. ^{99m}Tc(CO)$_3$-DAP-GSG-KCCYSL and ^{99m}Tc(CO)$_3$-(NαHis)Ac-GSG-KCCYSL exhibited high tumor-to-normal

organ uptake ratios. Radioactivity in the gastrointestinal (GI) tract of the mice was a result of excretion via the heptobiliary - GI route.

Specificity of tumor uptake of the radiolabeled peptides *in vivo* was further evaluated by carrying out competition experiments with cold Re labeled peptides. SPECT images showed that using the cold peptide ($[Re(CO)_3]$-DAP-GSG-KCCYSL or $[Re(CO)_3$-(NαHis)Ac] -GSG-KCCYSL) resulted in reduction of uptake of $^{99m}Tc(CO)_3$-DAP-GSG-KCCYSL and $^{99m}Tc(CO)_3$-(NαHis)Ac-GSG-KCCYSL (Figure 5C-D and 6C-D). The cold Re peptides saturated the available binding sites and prevented binding of the ^{99m}Tc peptides, which significantly reduced tumor visualization by SPECT. It is also evident from the images that the GI and kidney uptake of $^{99m}Tc(CO)_3$-DAP-GSG-KCCYSL and $^{99m}Tc(CO)_3$-(NαHis)Ac-GSG-KCCYSL were high in the blocked mice.

DISCUSSION

KCCYSL is a 6 amino acid peptide that was previously selected from a phage display library against the ECD of the tumor-associated ErbB-2 receptor [38]. The synthetic KCCYSL peptide exhibited high specificity for ErbB-2 and bound to ErbB-2 positive human breast and prostate carcinoma cells. Thus, KCCYSL has the potential to be developed into a cancer imaging or therapeutic agent targeting malignant cells overexpressing the ErbB-2 receptor.

In this study, we examined whether KCCYSL could be labeled with the popular SPECT imaging radionuclide ^{99m}Tc for use in imaging breast carcinomas *in vivo*. KCCYSL peptides were synthesized with a GSG spacer at their NH_2-terminal end to limit possible steric hindrance of the DAP or (NαHis)Ac chelators. The

$[^{99m}Tc(OH_2)_3(CO)_3]^+$ synthon can form stable bidentate (with DAP) or tridentate (with (NαHis)Ac) complexes. Radiolabeling of the R-GSG-KCCYSL peptides was successful at 75°C for 60 min with high radiochemical purity of more than 92%. Studies demonstrated high stability in pH 7.4 10 mM phosphate-buffered solution after 24 h.

Both $^{99m}Tc(CO)_3$-DAP-GSG-KCCYSL and $^{99m}Tc(CO)_3$-(NαHis)Ac-GSG-KCCYSL exhibited specific breast tumor uptake of 1.25 ±0.61 %ID/g and 0.75 ±0.40 %ID/g at 2 h post injection, respectively. Breast tumor uptake of $^{99m}Tc(CO)_3$-DAP-GSG-KCCYSL and $^{99m}Tc(CO)_3$-(NαHis)Ac-GSG-KCCYSL were higher than that of previously published ^{111}In-DOTA-GSG-KCCYSL with a tumor uptake of 0.66±0.11%ID/g at 2 h post injection [39]. $^{99m}Tc(CO)_3$-R-GSG-KCCYSL biodistribution studies indicated that the clearance of unbound radioactivity was rapid and proceeded primarily by the kidney, with some clearance *via* the GI tract. Tumor to blood and tumor to muscle ratios at 2 h for the two peptides were 0.75 and 6.95 for DAP and 0.58 and 6.92 for (NαHis)Ac, respectively. Based on the tumor uptake and tumor-to-normal tissue ratios from the biodistribution studies and the SPECT images, the $^{99m}Tc(CO)_3$-DAP-GSG-KCCYSL may have better potential as a tumor imaging agent than $^{99m}Tc(CO)_3$-(NαHis)Ac-GSG-KCCYSL. This could result from the fact that DAP forms bidentate complexes with ^{99m}Tc, leaving one coordination site with a free –OH group, while the (NαHis)Ac forms tridentate complexes with ^{99m}Tc with no free coordination sites. This free –OH group might reduce the hydrophobicity of the DAP-GSG-KCCYSL peptide.

Nonspecific binding of radiolabeled peptides in kidneys often occurs *in vivo* [77]. The amino acid composition of the KCCYSL peptide may enhance nonspecific kidney retention. The positively charged lysine as well as the two cysteine sulfhydryls in the

peptide probably contributed to prolonged renal radioactive uptake [56]. High levels of radioactivity retention in the kidneys could be attributed to the degraded radiolabeled peptide, produced by lysosomal degradation of the peptide with long residence times within renal cells and slow clearance from the lysosome [78-80]. A number of different methods have been investigated to reduce non-specific renal retention of radiolabeled peptides, including lysine or arginine infusion [81-84]; the use of colchicine [85] and Megalin [86]; introduction of glutamic acid into the peptide sequences [87]; co-infusion of the gelatine-based plasma expander Gelofusine and lysine [88-90]; and the use albumin fragments [91]. Gelofusine or lysine administration reduced kidney uptake by ~ 40% at all time points examined and the combination of Gelofusine and lysine resulted in a 62% inhibition of kidney uptake for radiolabeled DOTA-octreotide [89]. Numerous other studies have shown that the uptake of radiolabeled peptides in the kidney can be reduced by 40%-60% by infusion of amino acids before injection of radiolabeled peptides [92]. Gelofusine and lysine could be analyzed in future studies as a combination strategy to reduce renal uptake of radiolabeled KCCYSL peptides. Radioactivity in the lungs represented non-specific binding and may be due to the contribution of the blood pool radioactivity since the lungs are highly perfused [39]. For both $^{99m}Tc(CO)_3$-DAP-GSG-KCCYSL and $^{99m}Tc(CO)_3$-(NαHis)Ac-GSG-KCCYSL, there was no retention in the GI tract, as most of the radioactivity in the small intestine at early time points moved in to the large intestine or was excreted at 4 h post injection. An increased concentration of the radioactivity in the feces reflected the increased hydrophobicity of the $^{9m}Tc(CO)_3$-labeled peptide, resulting in high hepatobiliary clearance.

The SPECT/CT imaging studies indicated significant accumulation of $^{99m}Tc(CO)_3$-DAP-GSG-KCCYSL and $^{99m}Tc(CO)_3$-(NαHis)Ac-GSG-KCCYSL in the xenografted human breast carcinoma tumor. Radioactivity was also present in the kidney and GI tract, which serve as the routes of radiolabeled peptide excretion. Blocking studies in the SPECT/CT imaging confirmed that specific blockage, by addition of cold peptide, resulted in greatly reduced tumor uptake of $^{99m}Tc(CO)_3$-DAP-GSG-KCCYSL and $^{99m}Tc(CO)_3$-(NαHis)Ac-GSG-KCCYSL.

The facile production of the ^{99m}Tc synthon coupled with efficient radiolabeling of the peptide conjugates with compact bi- and tri- dentate chelators makes peptide labeling with $^{99m}Tc(CO)_3$ very attractive. The promise of rapid and reproducible ^{99m}Tc (I) peptide labeling is offset some what by the influence the chelated $^{99m}Tc(CO)_3$ moiety has on the chemical properties of short peptides and their *in vivo* pharmacokinetics. The ErbB-2-targeting peptide KCCYSL is a short hydrophilic peptide. In previous studies, conjugation of the peptide with the macrocyclic chelator DOTA via a GSG linker and subsequent labeling with ^{111}In yielded an ErbB-2-avid imaging agent with rapid renal and low hepatobiliary clearance, 6.45 ±0.69 %ID/g for kidney and 0.19 ±0.03 %ID/g for liver at 4 h [39]. The radiolabeling of the same peptide with $^{99m}Tc(CO)_3$-DAP or $^{99m}Tc(CO)_3$-(NαHis)Ac resulted in an ErbB-2 imaging agent with high hepatobiliary and renal clearance, such as 4.39 ±1.89 and 1.84 ±0.52 %ID/g for DAP and 4.37 ±0.59 and 1.53 ±0.22 %ID/g for (NαHis)Ac for kidney and liver respectively at 4 hours. An increase in the hydrophobicity of the $^{99m}Tc(CO)_3$ complexes resulted in prolonged blood clearance, higher amounts of radioactivity in the liver and intestines compared to the ^{111}In- DOTA complex. Higher levels of radioactivity in the guts of mice injected with the $^{99m}Tc(CO)_3$

complexes are evident in SPECT images and would preclude identification of tumors in the liver and GI. Similar biodistribution and hepatobiliary/GI excretion results were reported for $^{99m}Tc(CO)_{3}$- labeled gastrin releasing peptide [65-66] $^{99m}Tc(CO)_3$-labeled RGD (34) and $^{99m}Tc(CO)_3$-labeled MSH (35), although the pyrazolyl chelator [93-94] appears to be slightly more hydrophilic that the DAP or NαHis chelators. While the $^{99m}Tc(CO)_3$ complex is compact and not likely to cause steric hindrance of peptide for target binding, the hydrophobicity of the $^{99m}Tc(CO)_3$ complex must be improved if it to be successful in producing small peptide imaging agents. Modification of the $^{99m}Tc(CO)_3$ chelators or addition of a hydrophilic linker between the targeting peptides and the $^{99m}Tc(CO)_3$ complex may offset its hydrophobicity.

TABLE 1. Biodistribution of $^{99m}Tc(CO)_3$-DAP-GSG-KCCYSL, $^{99m}Tc(CO)_3$-(Nα His)AcGSG-KCCYSL in female SCID mice bearing MDA-MB-435 human breast carcinoma tumors. The data are presented as percent injected dose per gram of tissue and percent injected dose (Mean±SD, n = 4).

Compounds	$^{99m}Tc(CO)_3$-DAP-GSG-KCCYSL					$^{99m}Tc(CO)_3$-(Nα His)Ac- GSG-KCCYSL				
Tissue	1 h	2 h	2 h block	4 h	24 h	1 h	2 h	2 h block	4 h	24 h
	Percent Injected Dose/Gram (%ID/g)					Percent Injected Dose/Gram (%ID/g)				
Tumor	1.67±0.16	1.25±0.61	0.88±0.27	0.88±0.12	0.30±0.06	0.76±0.13	0.75±0.40	0.59±0.14	0.33±0.08	0.16±0.02
Blood	2.65±0.26	1.65±0.34	1.41±0.42	1.29±0.28	0.19±0.05	1.66±0.08	1.30±0.65	1.30±0.14	1.05±0.15	0.33±0.05
Heart	0.99±0.10	0.64±0.12	0.52±0.15	0.51±0.12	0.13±0.03	0.60±0.06	0.43±0.22	0.42±0.01	0.41±0.07	0.19±0.02
Lung	4.35±0.29	1.68±0.28	2.51±2.08	2.19±0.33	0.30±0.07	1.21±0.11	3.80±2.00	2.48±0.35	0.78±0.08	0.39±0.02
Liver	3.92±0.26	2.32±0.43	1.96±0.49	1.84±0.52	0.35±0.08	2.01±0.08	7.81±3.68	5.04±0.74	1.53±0.22	0.75±0.09
Spleen	0.71±0.10	0.50±0.07	0.43±0.12	0.42±0.08	0.11±0.04	0.35±0.01	0.95±0.72	1.13±0.17	0.26±0.06	0.20±0.04
Stomach	0.75±0.22	0.49±0.07	0.63±0.36	0.67±0.19	0.10±0.04	0.94±0.83	6.34±2.14	6.30±1.32	1.32±1.67	0.16±0.06
Intestines	2.87±0.32	3.91±0.92	3.16±1.26	4.35±1.22	0.20±0.04	5.29±0.84	8.39±3.72	6.51±0.51	6.36±1.47	0.31±0.07
Kidneys	8.43±0.82	8.24±0.94	7.00±0.48	4.39±1.89	0.91±0.24	9.93±0.75	5.49±2.69	4.55±0.22	4.37±0.59	1.51±0.17
Brain	0.11±0.03	0.06±0.02	0.05±0.01	0.06±0.03	0.01±0.00	0.05±0.00	0.04±0.02	0.04±0.01	0.03±0.01	0.01±0.00
Muscle	0.31±0.05	0.18±0.03	0.17±0.07	0.15±0.04	0.04±0.02	0.18±0.04	0.11±0.03	0.12±0.01	0.10±0.02	0.06±0.01
Bone	0.32±0.12	0.24±0.10	0.20±0.09	0.18±0.06	0.06±0.02	0.14±0.01	0.27±0.14	0.40±0.03	0.11±0.02	0.06±0.02
Skin	0.86±0.22	0.49±0.15	0.32±0.13	0.42±0.07	0.09±0.04	0.41±0.16	0.46±0.18	0.38±0.04	0.15±0.04	0.13±0.05
	Percent Injected Dose (%ID)					Percent Injected Dose (%ID)				
Small intestine	5.82±0.38	3.26±1.53	3.31±0.41	1.55±0.49	0.19±0.06	11.80±0.84	10.71±7.44	5.38±2.68	1.46±0.76	0.27±0.06
Large intestine	0.32±0.04	4.03±1.16	2.03±1.01	6.76±1.09	0.35±0.08	1.01±1.39	3.88±4.18	5.83±4.25	12.25±2.02	0.38±0.12
Urine	73.31±1.72	79.39±2.28	80.06±7.29	81.26±3.30	97.00±0.36	72.25±2.62	65.68±12.77	72.10±2.13	79.58±2.17	96.08±0.62
	Uptake Ratio of Tumor/Normal Tissue					Uptake Ratio of Tumor/Normal Tissue				
Tumor/blood	0.63	0.75	0.62	0.68	1.55	0.46	0.58	0.46	0.32	0.47
Tumor/lung	0.38	0.74	0.35	0.4	1	0.63	0.2	0.24	0.42	0.41
Tumor/liver	0.43	0.54	0.45	0.48	0.85	0.38	0.1	0.12	0.22	0.21
Tumor/kidneys	0.20	0.15	0.13	0.20	0.33	0.08	0.14	0.13	0.08	0.10
Tumor/muscle	5.31	6.95	5.19	5.70	6.83	4.32	6.92	4.95	3.39	2.84

The data are presented as percent injected dose/gram (Mean±SD, n = 4).

A.

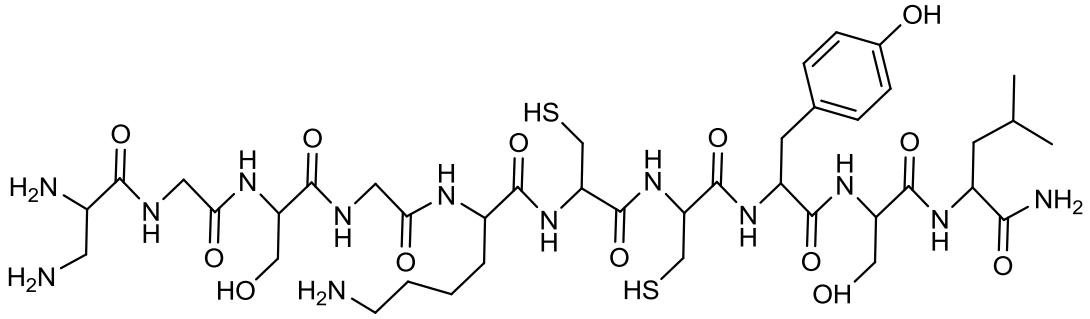

B.

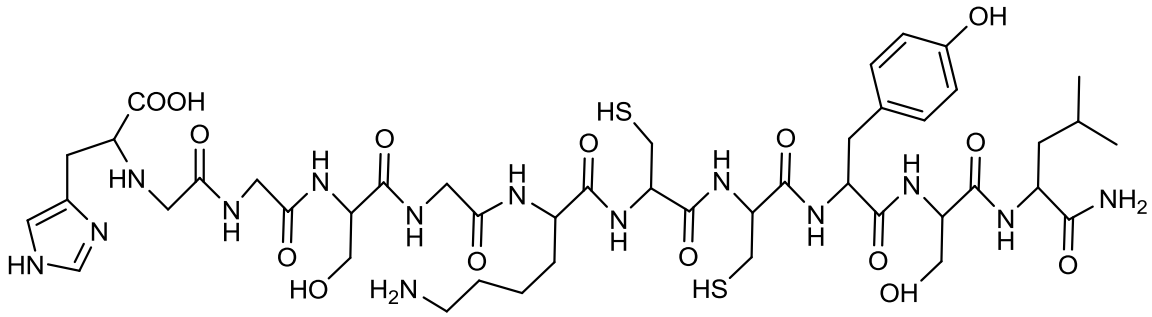

Fig. 1. The chemical structures of (A) DAP-GSG-KCCYSL and (B) (NαHis)Ac-GSG-KCCYSL.

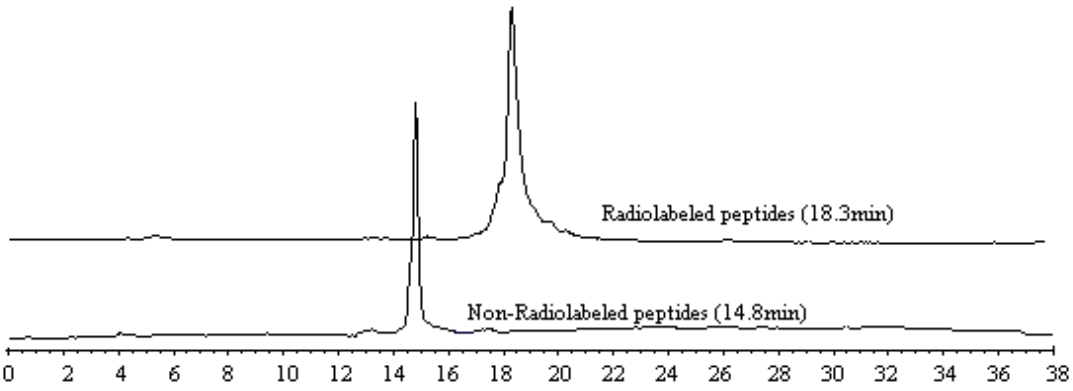

Fig. 2. RP-HPLC elution profile of DAP-GSG-KCCYSL and (NαHis)Ac-GSG-KCCYSL peptides with and without $^{99m}Tc(CO)_3$ radiolabeling. Both non-radiolabeled peptides had a retention time of 14.8 min, while the radiolabeled peptides had a retention time of 18.3 min.

A

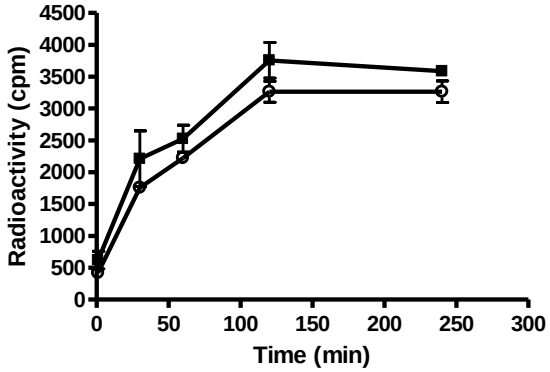

B

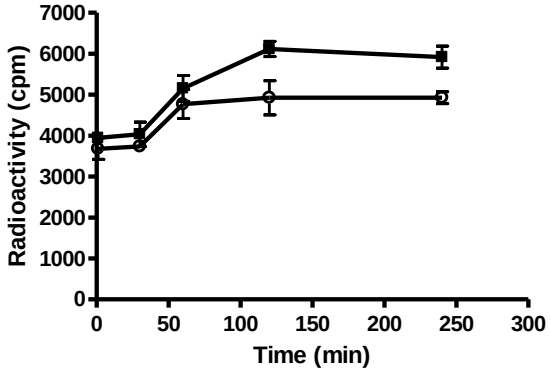

Fig. 3. *In vitro* ErbB-2 receptor binding of $^{99m}Tc(CO)_3$-(NαHis)Ac-GSG-KCCYSL (A) and $^{99m}Tc(CO)_3$-DAP-GSG-KCCYSL (B) peptides. Approximately 1.25 x 10^6 cells per well were incubated at various time intervals with 8 x 10^4 cpm of radiolabeled peptide. For both (NαHis)Ac-GSG-KCCYSL (A) and DAP-GSG-KCCYSL (B) higher binding was observed for human breast carcinoma MDA-MB-435 cells (■) than for human leukemia K562 cells (○).

A

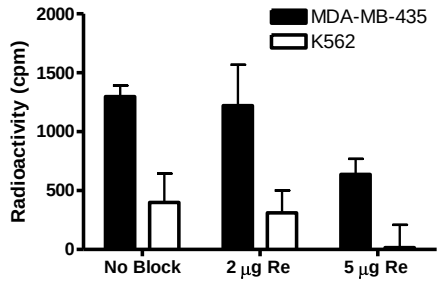

B

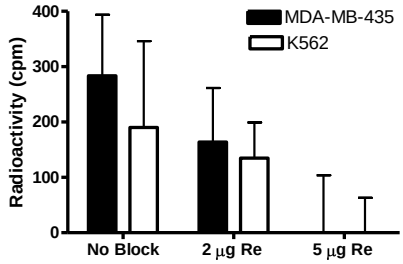

Fig. 4. In *vitro* blocking studies with $^{99m}Tc(CO)_3$-DAP-GSG-KCCYSL (A) and $^{99m}Tc(CO)_3$-(NαHis)Ac -GSG-KCCYSL (B). Approximately 1.25 x 10^6 cells per well were incubated for 2 hours with 8 x 10^4 cpm of radiolabeled peptide and various amounts of cold Re labeled peptide. After the nonspecific binding of the radiolabeled peptide to the negative cell line was set to zero, the blocking for $^{99m}Tc(CO)_3$-DAP -GSG-KCCYSL was reduced by 42% and 100%, for 2 and 5 μg of cold Re labeled peptide respectively and the blocking for ^{99m}Tc-(NαHis)Ac -GSG-KCCYSL was reduced by 6% and 51%, respectively.

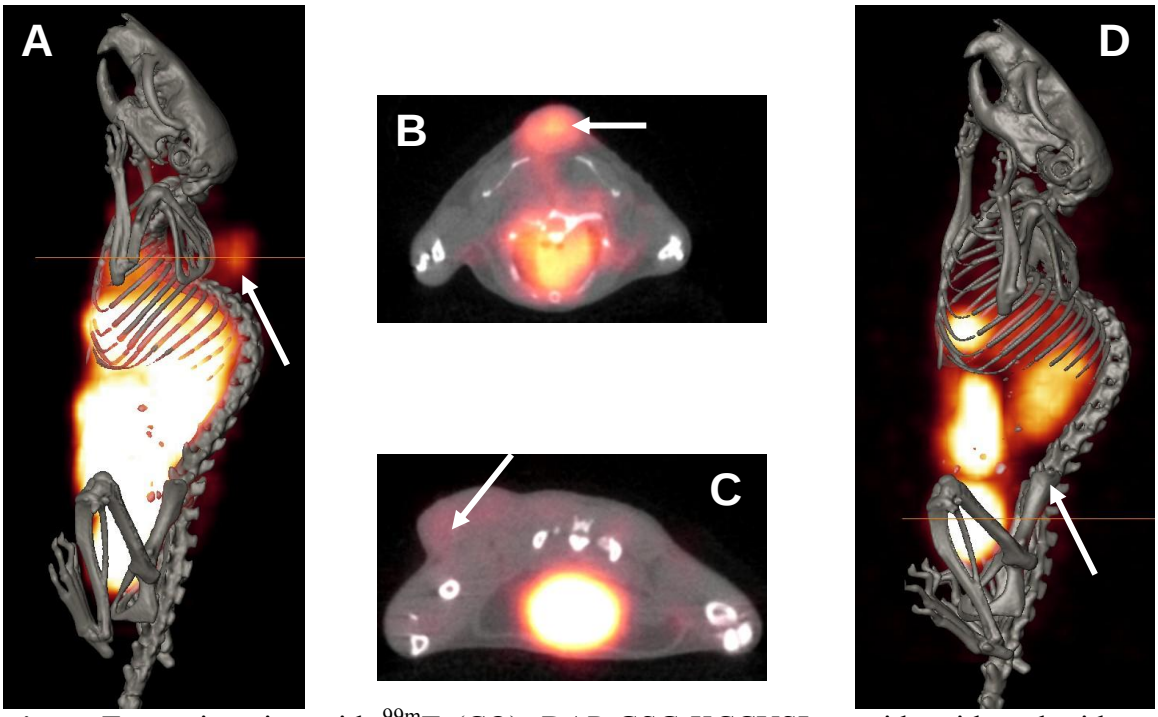

Fig. 5. Tumor imaging with $^{99m}Tc(CO)_3$-DAP-GSG-KCCYSL peptide with and without the presence of the cold competator Re-DAP- GSG-KCCYSL. SCID female mice bearing MDA-MB-435 human breast carcinoma cells were injected in the tail vein with 500 µCi of $^{99m}Tc(CO)_3$-DAP-GSG-KCCYSL and imaged live at 2 hours post injection in a micro SPECT scanner. The SPECT images were fused with conventional microCT images to confirm regions of increased peptide uptake, resulting in whole body (A) and transaxial (B) images. 100 µg of cold competitor Re-DAP-GSG-KCCYSL, to block uptake of ^{99m}Tc-peptide, was injected 15 min before injection of 500 µCi of $^{99m}Tc(CO)_3$-DAP-GSG-KCCYSL intravenously into SCID female mice bearing MDA-MB-435 human breast carcinoma cells. Similar imaging in a microSPECT scanner resulted in whole body (D) and transaxial (C) images.

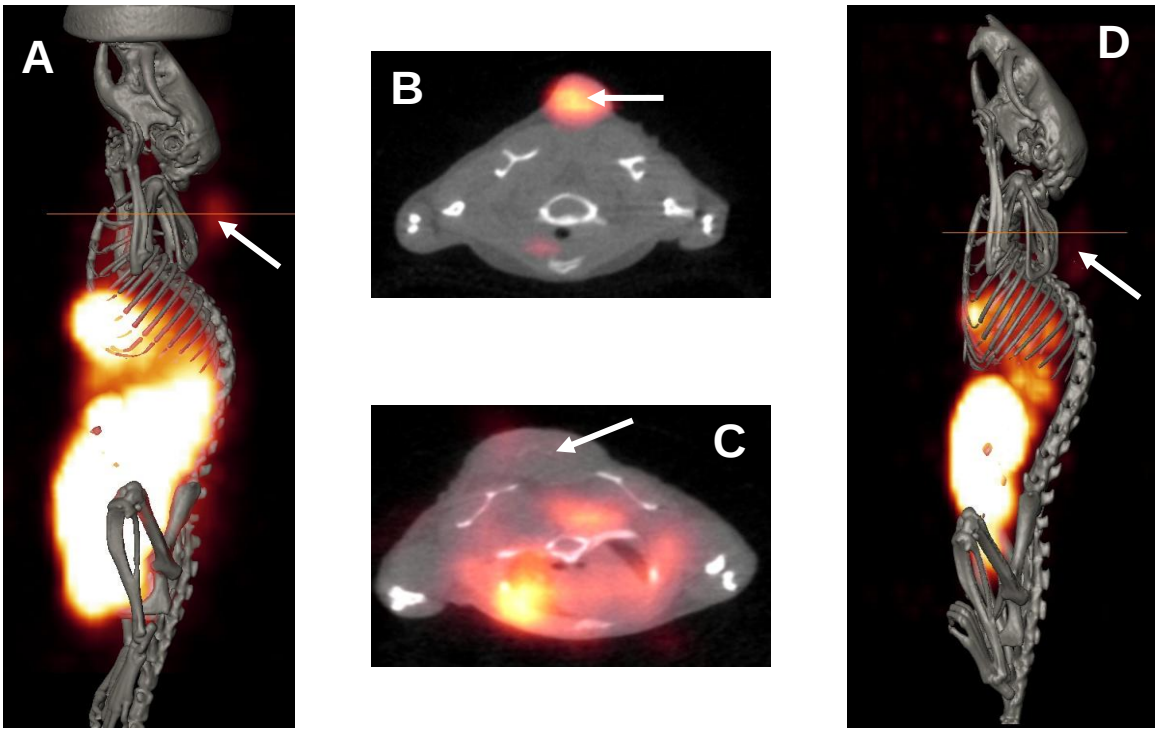

Fig. 6. Tumor imaging with $^{99m}Tc(CO)_3$-(NαHis)Ac -GSG-KCCYSL peptide with and without the presence of the cold competator Re-(NαHis)Ac - GSG-KCCYSL. SCID female mice bearing MDA-MB-435 human breast carcinoma cells were injected in the tail vein with 500 µCi of $^{99m}Tc(CO)_3$-(NαHis)Ac -GSG-KCCYSL and imaged live at 2hours post injection in a micro SPECT scanner. The SPECT images were fused with conventional microCT images to confirm regions of increased peptide uptake, resulting in whole body (A) and transaxial (B) images. 100 µg of cold competitor Re-(NαHis)Ac - GSG-KCCYSL, to block uptake of ^{99m}Tc-peptide, was injected 15 min before injection of 500 µCi of $^{99m}Tc(CO)_3$-(NαHis)Ac -GSG-KCCYSL intravenously into SCID female mice bearing MDA-MB-435 human breast carcinoma cells. Similar imaging in a microSPECT scanner resulted in whole body (D) and transaxial (C) images.

CHAPTER 3- GALECTIN-3 PEPTIDE CHARACTERIZATION

INTRODUCTION

Antibodies (Abs) are currently the most common targeting method for the radioimaging of tumors [24, 95]. While whole Abs are useful *in vitro*, the large size results in *in vivo* problems such as long biodistribution times, slow liver clearance and tumor penetration [27]. Smaller Ab fragments (Fab) have been produced to circumvent these problems, and as the clearance is improved, the targeting affinity is often reduced [96]. Peptides have been shown to offer advantages over Abs and Fabs because of their rapid blood clearance, increased diffusion, non-immunogenic nature, and ease of synthesis [75, 97].

While other receptor systems are being used for targeted cancer imaging agents, the potential of carbohydrate-lectin complexes remains relatively unexplored. Tumor growth and metastasis are processes that involve cancer cell movement and adhesion that allow the cancer cells to leave the primary tumor, move into vasculature and from the vasculature move into new sites where secondary tumors occur [98]. One of the most important lectins, or sugar binding proteins, involved in cancer cell adhesion is gal-3. Gal-3 is in the galectin family of lectins that bind β-galactose residues [14], and is expressed in several types of cancer including breast [15-16]. The major ligand for gal-3 found on tumors is the Thomsen-Friedenreich antigen (TF), which is a galactose β1-3 N-acetylgalactosamine disaccharide expressed on breast cancer and up to 90% of all cancers [17-18]. On healthy cells, the TF antigen is masked by sialic acid, and therefore it does not interact with gal-3 [99]. The gal-3-TF interaction increases cancer cell adhesion by cross-linking carbohydrate-mediated antigens on cells expressing these antigens. The

increased adhesion is an early step in the metastatic cascade. Thus, the ability to image gal-3-TF interactions may be a valuable early breast cancer diagnostic.

It has been shown that TF promotes the expression of gal-3 in breast cancer, and other cancer cells including prostate [19]. Also, TF induces the expression of gal-3 in endothelial cells, and when tumor cells are stimulated with TF, endothelial gal-3 redistributes to sites in contact between the tumor and endothelial cells, making the gal-3-TF interactions a potential novel approach for the imaging of breast cancer cells [18-21].

Phage display is a technique that uses targets, such as the biomarker gal-3, to identify random peptide sequences that bind to specific targets. A phage-display "library" is a mix of filamentous phage with foreign peptides on their surface and the coding sequence for the peptide in the viral DNA of the phage, which can be used to survey for phage that displayed peptide binds to a specific target molecule. Our laboratory has been successful in selecting tumor targeting peptides from *in vitro* and *in vivo* phage display. Normal development of cancer imaging or therapeutic compounds for clinical use has traditionally relied on isolation of products from natural extracts, screening compound databases, structure-based rational drug design, or antibody engineering. This phage display technique uses phage libraries to identify compounds that interact with the desired target, and then subsequent rounds of affinity selection can yield rare specific binders from an enormous collection of molecules. Previously, a peptide antagonist of gal-3 was identified from phage display libraries which blocked TF-gal-3 interactions and reduced breast cancer cell adhesion *in vitro* and tumor growth *in vivo* [44]. This result identifies a potential peptide for the imaging of breast cancer. It was therefore hypothesized that understanding the key residues of this peptide will be

beneficial to the understanding of binding between this peptide and gal-3 protein. Once the key residues are understood, then binding can be maximized with an ideal sequence in hopes that future work will be done to determine the best chelator in order to create a breast cancer imaging agent.

The anti-gal-3 peptide is G3-C12 (ANTPCGPYTHDCPVKR) and the key binding residues of this peptide will be determined using point mutations of each residue of the G3-C12 sequence. Ala substitutions will be made at each residue, with the residue that was originally Ala replaced with Ser. Point mutations will allow us the ability to determine which individual amino acids are important in the interaction between the peptide and gal-3. This will give information about the binding process between anti-gal-3 peptide G3-C12 and gal-3. Also, point mutation sequences will help determine which positions might be better for chelator attachment. These interactions will be studied using two methods, ELISA and cell binding assays. For ELISAs, anti-gal-3 peptide G3-C12 and mutants will be immobilized on a plate and soluble peptides covalently modified with biotin interact with the bound gal-3. Gal-3 protein and peptide interaction will be detected via the biotin binding protein Streptavidin, which is covalently attached to horseradish peroxidase (HRP). HRP is commonly used in colorimetric assays. G3-C12 peptide and mutant peptides abilities to bind different cell types, positive and negative, will be tested via confocal microscopy. Soluble peptides covalently modified with biotin interact with the bound cells fixed to microscope slides. Binding will be detected with Streptavidin covalently attached to Oregon Green for fluoresecent imaging. Using the aforementioned two methods will yield results showing the importance of each amino acid residue to the binding of G3-C12 peptide and gal-3 protein. The results will prove

my hypothesis that understanding the key residues of this peptide will be beneficial to the development of a breast cancer imaging agent.

MATERIALS AND METHODS

2.1 Chemicals and Reagents

All peptide synthesis reagents were purchased from Novabiochem (San Diego, CA) or Genzyme (Cambridge, MA). All other chemicals were purchased from Sigma Chemical Company (St. Louis, MO), unless otherwise stated. Cell culture reagents were purchased from Invitrogen (Carlsbad, CA).

2.2 Cell Lines and Cell Culture

Human breast carcinoma cell line MDA-MB-435 and prostate cancer cell line PC3 were received from American Type Tissue Culture (Manassas, VA). The cells were maintained as monolayer cultures in RPMI 1640 Custom media (Invitrogen, St. Louis, MO) with 10% FBS and 0.06 mg/mL gentamycin. Cultures were maintained at 37°C in a 5% CO_2 humidified incubator.

2.3 Peptide Synthesis

Peptides were synthesized in a model 396 multiple peptide synthesizer (Advanced Chem Tech, Louisville, KY) using solid-phase Fmoc chemistry. Cleavage and side chain deprotection were achieved by treating the resin with 87.5% trifluoroacetic acid / 2.5% thioanisole / 2.5% phenol / 2.5% water / 2.5% ethandithiol / 2.5% triisopropylsilane. The peptides were purified by semipreparative High Performance Liquid Chromatography (HPLC) (Beckmann Coulter, Fullerton, CA). Crude and pure peptide preparations were

characterized by Liquid Chromatography-Mass Spectrometry (LC-MS) (Thermo Finnigan, San Jose, CA).

2.4 Galectin-3 Purification

His tagged Gal-3 was expressed in *E. coli* from the pET 3 vector. 2 L of LB cultures were inoculated with E. coli and were grown at 37 ºC with 225 revolutions per minute (rpm) shaking with antibiotic concentration of 1µ/mL ampicillin until an optical density of 0.45 at 595 nm was detected using a Cary 50 Bio UV-Visible Spectrophotometer from Varian. Phenylmethanesulfonylfluoride (PMSF) was added to make a final concentration of 100 µg/mL and isopropyl-ß-D-thiogalactopyranosid (IPTG) was added to a final concentration of 1 mM and cells were grown at 37 ºC with shaking for 4 additional hours. PMSF was added to deactivate proteases from digesting proteins after cell lysis and IPTG was added to induce gal-3 production. After 4 hours, the cells were spun down to a pellet, and the supernatant was discarded. The pellet was resuspended in ~40 mL lysis buffer (50 mM NaH_2PO_4, 300 mM NaCl, 10 mM imidazole). A protease inhibitor tablet, Roche Complete Mini, was added and cells were iced for 30 min. Cells were then sonicated for 20 sec bursts with 20 sec ice breaks in between sonications repeating five times The lysed cells were spun down at 12,000 rpms for 20 min and the supernatant was retained.

Purification was performed using a Ni NTA column with 10 mL of column slurry per 40 mL lysate supernatant. The slurry and supernatant were incubated in a 50 mL conical tube shaking on ice for 60 min. Next, the slurry and supernatant were loaded onto an empty Biorad column and washed with 50 mL wash buffer (50 mM NaH_2PO_4, 300 mM NaCl, 20 mM imidazole) 2 times. The protein was eluted with elution buffer

(50 mM NaH_2PO_4, 300 mM NaCl, 250 mM imidazole) 4 times using 6 mL each. Centriprep YM-10 columns were used to remove excess salt from protein and concentrate the protein sample. The columns were loaded with the eluted protein and were spun at 3000 g for 10 min periods, continuing until the retentate volume was ~2 mL, making sure to remove the flow through at each step. Buffer exchange was performed *via* this column when 15 mL of PBS was added to each column and spun again until retentate volume was ~2 mL. This exchange step was repeated 3 times with the final concentrated protein found in rententate solution left in centriprep columns.

2.5 Enzyme-linked immunosorbent assay (ELISA)

Purified gal-3 protein (0.5 μg) was preabsorbed to a 96-well plate overnight at 4º C then blocked for 2 h with BSA (6%). After extensive washing with Tris-Buffered Saline Tween-20 (TBST), biotinylated anti-gal-3 peptides (G3-C12, scrambled control, and Ala point mutation sequences) were added (100 μL of 1μM concentration in TBS) and incubated for 1 h at room temperature. After a TBST wash, HRP-Streptavidin (100 μL of 1:1000 in TBS) was added and incubated for 1 h at room temperature. After washing in TBST, colorimetric detection of bound gal-3 peptide was determined by development using room temperature 2,2'-azino-bis (3-ethylbenzthiazoline-6-sulfonic acid). The developer reacts with the peroxidase in the HRP, and the end product is a green solution, which can be easily measured using a spectrophotometer. The absorbance at 405 nm was recorded. Negative controls included no capture gal-3 protein in the wells, no peptide, and no streptavidin wells. A positive control included biotinylated gal-3 protein captured on certain wells.

2.6 Cell-surface Binding

1×10^4 cells of each dispersed cell suspension (phosphate buffered saline, pH 7.4, 4% formaldehyde) were dried onto a microscope slide and blocked (6% BSA solution for 2 h at room temperature). After washing 3 times at 5 min each TBST the slides were incubated with biotinylated peptide solutions (20 μM in 10 mM Tris, pH 7.5, 1% BSA) for 1 h at RT. After washing with TBST, binding was detected by using Oregon Green Streptavadin (Molecular probes, Eugene, OR) (10 μg/ml in 10 mM Tris, pH 7.5, 1% BSA) for fluorescent imaging for 1 h at RT in the dark. After a final wash with TBS, a cover slip was attached. Laser scanning confocal microscopy was performed using a Nikon Eclipse TS100 microscope.

RESULTS

3.1 Peptide Synthesis

The sequences of the G3-C12 peptide and all the point mutation sequences are shown in Table 2. Point mutation replacements of native amino acids with Ala were created and the point mutation to the small CH_3 group of Ala reduces the size of the amino acid side chain. One amino acid was already Ala so a mutant was created replacing the Ala with Ser. Lastly, a double replacement of both Cys with Ala was created. For use as a negative control, a scrambled point mutation sequence of G3-C12 was created. Cell binding experiments were performed with G3-C12 peptide (ANTPCGPYTHDCPVKR) and the negative control sequence peptide (NTPADGPYTHDAPVKR) bound to gal-3 positive and negative cell lines. Confocal microscopy was performed on Oregon green labeled streptavadin bound to biotinylated peptide on the surface of the cells and is shown in Fig 7. As expected, the data shows a

high signal level of anti-gal-3 G3-C12 peptide with the gal-3 positive cell line, MDA-MB-435, indicating good binding between G3-C12 and the gal-3 protein. In comparison, there is a very low signal level for G3-C12 peptide and the gal-3 negative cell line, indicating very low binding of the peptide to cells not expressing gal-3. The modified negative control sequence also shows low signal for peptide and gal-3 positive cell line and a very low signal for peptide and gal-3 negative cell line. These combined results show the utility of G3-C12 for the targeting of gal-3 and the use of scrambled peptide for abolishing the binding. Overall, the scrambled peptide result indicates specificity of binding for the gal-3 protein.

3.2 ELISA

Point mutations of Ala, replacement of Ala with Ser, and double Cys to Ala mutants were made as shown in Table 2. Once all mutant peptides were synthesized, their binding potentials for gal-3 were studied using ELISA. Immobilized gal-3 (0.5 ug) was interacted with biotinylated peptide solutions (1μM) of G3-C12, all point mutations, and scrambled peptide. The binding potential was determined using fixed gal-3, bound biotinylated peptide, HRP-Streptavidin and 2,2'-azino-bis (3-ethylbenzthiazoline-6-sulfonic acid) as developer. HRP is a horseradish peroxidase that reacted with the developer, which resulted in a green product whose absorbance at 405 nm was measured. This allowed for the colorimetric detection of the amount of HRP, thus the amount of steptavidin and bound biotinylated peptide within each well. Wells with immobilized biotinylated gal-3 protein acted as positive control for the secondary and developer. The absorbance at 405 nm was determined using a 96 well plate spectrometer. The absorbances found in wells with no gal-3 capture were treated as blanks.

The absorbance values were calculated as a percentage of G3-C12, with the value of G3-C12 at 100.0%. Results are shown in Fig. 8 and are arranged in both sequence order and order of percent absorbance compared to original G3-C12. The student t-test was performed for each data set to determine the significance of the values, and a * was marked on Figure 8 for each mutated peptide sequence that was determined to have statistical significance by having a p value of lower than 0.05.

Few mutants were found to be statistically insignificant by having p-values of higher than 0.05. These mutants held similar binding ability as the original G3-C12, with His10Ala, Pro13Ala, and Arg16Ala having bindings of 104-100% of that of G3-C12. Results suggest that the modification of these residues does not affect binding significantly, indicating that these residues are not important in binding. The highest level of binding was found with mutant Val14Ala, which resulted in 116% of the original G3-C12. This mutant had a p-value of 0.002 indicating statistical significance in the difference between the original G3-C12 and the Val14Ala mutant. This result indicates that this residue is important for binding between G3-C12 and gal-3, and that changing the residue resulted in better binding than the original sequence.

Most point mutations resulted in lower binding potential than the original G3-C12, with 5 residues in which a mutation resulted in significant reduction in binding, to lower than 60% of original binding strength. These mutations were Ala1Ser with 40%, Cys5Ala 50%, Gly6Ala 58%, Cys12Ala 55% of G3-C12. They were shown to be statistically significant differences with p-values ranging from 0.001 to 3.2 E-6. These results suggest that these residues are important for binding between G3-C12 and gal-3, and that changing these residues resulted in weaker or less binding than the original

sequence. The mutation that provided the greatest difference in binding strength was the double Cys5&12Ala mutant which had only 19% of the original C3-G12 while the negative control peptide had only slightly less with 16%. Double Cys5&12Ala mutant was also shown to be the most statistically significant of all mutations with a p-value of 9.6 E-7. This result indicates that both residue 5 and 12 are important for binding and modification of both residues results in decreased binding interactions. Overall, the key residues that resulted in lowered binding which must be important for binding were Ala1Ser, Cys5Ala, Gly6Ala, and Cys12Ala and so the binding site must include these key residues.

3.3 Cell-surface Binding

MDA-MB-435 human breast and PC3 human prostate cancer cell lines were used for cell binding assays. MDA-MB-435 breast carcinoma cells are positive for gal-3 while PC3 were used as the negative control cell line because they do not express gal-3 [100]. A 20 μM peptide concentration was determined in previous laboratory work to be the desired concentration for cell binding studies [44]. G3-C12 peptide at 20μM bound to MDA-MB-435 cells but not to PC3 cells, indicating the selectivity of the peptide for gal-3. Binding was studied for all sequences described in Table 2. Using the software Image J, regions of interest were set for each image and the intensity of the fluorescence was measured. These values were normalized to G3-C12 binding to MDA-MB-435 with the G3-C12 signal being 100% intensity and were graphed both by sequence order and intensity strength, shown in Figure 10. The highest intensity mutation was Val14Ala with 87.7%, which also exhibited high binding in the ELISA assay. Mutations that provided the highest differences in binding strength, found to have less than 40% of G3-

C12 signal, were Pro13Ala (39.5%), Cys12Ala (38.3%), Ala1Ser (37.0%), Arg16Ala (34.6%), and Lys15Ala (28.4). The mutation that provided the greatest difference was the double mutant Cys5&12Ala with 27.2% of the original C3-G12 signal while the negative control peptide had 28.4%. Overall, the key residues that resulted in lower binding which must be important for binding were Ala1Ser, Cys5Ala, Cys12Ala, Pro13Ala, Lys15Ala, and Arg16Ala. Several of these residues were also identified in the ELISA to be key residues. This data further bolsters the idea that the binding site for gal-3 involves these residues, specifically residue positions 1, 5 and 12-16.

DISCUSSION

The creation of Ala point mutation peptide sequences of G3-C12 (ANTPCGPYTHDCPVKR) was done to study the effect of each amino acid residue in the peptide for gal-3 binding potential. A scrambled point mutation sequence was found to have reduced gal-3 binding, and thus this sequence has use as a negative control. The residues that are different in the scramble and original sequence are potentially the residues that interact with anti-gal-3 G3-C12. As residues 1-5 and 12 are the only residues different from the original G3-C12, it would appear that these 6 residues are important in peptide binding to gal-3. These results agree with the ELISA and cell binding data and show that residue 1, 5, and 12 are of key importance for the binding of G3C-12 and gal-3 protein.

There are several residues of interest based on ELISA data. The point mutation of Val14Ala was the only mutation that resulted in greater cell binding signals with 116% of G3-C12 signal for ELISA data. This mutation results in the removal of the larger valine

branched 3 carbon side chain and replacement with an alanine single methyl group. It is likely the three dimensional arrangement of the peptide sequence has steric hindrance alleviated by the replacement with the Ala residue, which results in improved interaction between gal-3 and peptide.

Besides the residue that increased binding efficiency, the mutations that decreased the binding efficiency also provide information about the key residues. Other key residues investigated include Ala1Ser, Cys5Ala, and Cys12Ala, which resulted in the large decreases in binding by approximately half. However, the greatest change was the double mutant of Cys5&12Ala with reduction of the binding affinity to 19% of the original C3-G12 signal based on ELISA data. The thiol side chain group of cysteine contains sulfur, which can interact with another thiol group to form a disulfide bridge. There is a potential that the two residues with thiol groups interact together to form a bridge important for binding to gal-3 protein. Peptides with 1 thiol group such as the Cys5Ala or Cys12Ala, instead of 2 thiol groups on the original peptide, would have their disulfide bridges disturbed, which would account for the 50% reduction in binding. This ELISA study indicates that residues 1-Ala, 5-Cys, and 12-Cys are of importance for binding with specific focus on the potential disulfide bonds from residue 5 and 12. The GSG linker is attached at residue 15, which in the ELISA did have reduced binding when point mutated but it was not identified to be one of the key residues. This linker binding selection was more optimal than the option to bind the linker at the N-terminus residue 1, since residue 1 was identified to be a key binding residue. The placement of the GSG linker at residue 1 could result in significant reduction of binding, since the linker would reduce the available space around the binding site at residue 1.

The cell binding study illustrated that both G3-C12 and its various mutants did preferentially bind to cells expressing gal-3 over cells not expressing gal-3. This result indicates the potential of this peptide as an imaging agent for tumors composed of breast cancer cells. Analysis showed that Val14Ala had the highest level of binding compared to the original G3-C12. Other key residues that showed a decrease in binding included Ala1Ser, Cys12Ala, Pro13Ala, Lys15Ala, Arg16Ala, and Cys5&12Ala. This shows that the residues of importance are 1, 5 and 12-16, with particular importance on the Cys residues at position 5 and 12. These results align with ELISA results, particularly the importance of the positions 1, 5, and 12.

Experiments with the scrambled control peptide and the point mutations peptides have shown a number of important key residues in the G3-C12 sequence. While the Val at residue 14 is important for binding, the change to Ala increases the binding with gal-3 protein and further study might be warranted for this Val14Ala mutant. The Ala1Ser also resulted in decreased binding, indicating that the hydroxyl side group of serine was affecting binding. Residues 5 and 12, the two cysteine residues, show importance for binding, as removal decreases binding and the double mutant binding level is further decreased.

One experiment that would provide further information about the mechanism of binding between gal-3 and anti-gal-3 peptide G3-C12 would be a fluorescence quenching experiment, measuring the reaction between fixed amounts of gal-3 protein and varying amounts of peptide. Gal-3 protein would be labeled with a fluorescent donor and peptides with a fluorescent quencher. When gal-3 protein and peptide interact, the quencher attached to the peptide would reduce the fluorescent light emitted from the gal-

3 protein, which would indicate the strength of the interaction. The fluorescence change as the peptide concentration changes would allow for the calculation of the K_d value, or the equilibrium dissociation constant. The K_d would more accurately reflect the strength of the interaction between peptide and protein and studying the various mutant peptides would give insight into the binding mechanism.

When more information is known about the binding mechanism and an ideal sequence has been identified, then studies can be performed to determine a proper chelator for the G3-C12 peptide. Once the correct chelator has been developed, then radiolabeling, binding, and *in vivo* studies as done in Chapter 2 with KCCYLS peptide and ErbB-2 could be done for G3-C12 peptide and gal-3 protein. Ultimately, a cancer imaging agent could be created using the peptide G3-C12 which would be used to image small cancer tumors and hopefully diagnose cancer at an earlier stage so that treatment will be successful.

Table 2. Galectin-3 selected peptide G3C12 and Ala point mutation peptides and scrambled control peptides with highlighted changes from original G3-C12 peptide.

Code	Sequence
G3-C12	A N T P C G P Y T H D C P V K R
Ala1Ser	**S** N T P C G P Y T H D C P V K R
Asn2Ala	A **A** T P C G P Y T H D C P V K R
Thr3Ala	A N **A** P C G P Y T H D C P V K R
Pro4Ala	A N T **A** C G P Y T H D C P V K R
Cys5Ala	A N T P **A** G P Y T H D C P V K R
Gly6Ala	A N T P C **A** P Y T H D C P V K R
Pro7Ala	A N T P C G **A** Y T H D C P V K R
Try8Ala	A N T P C G P **A** T H D C P V K R
Thr9Ala	A N T P C G P Y **A** H D C P V K R
His10Ala	A N T P C G P Y T **A** D C P V K R
Asp11Ala	A N T P C G P Y T H **A** C P V K R
Cys12Ala	A N T P C G P Y T H D **A** P V K R
Pro13Ala	A N T P C G P Y T H D C **A** V K R
Val14Ala	A N T P C G P Y T H D C P **A** K R
Lys15Ala	A N T P C G P Y T H D C P V **A** R
Arg16Ala	A N T P C G P Y T H D C P V K **A**
Cys5&12Ala	A N T P **A** G P Y T H D **A** P V K R
Negative Control	**N T P A D** G P Y T H D **A** P V K R

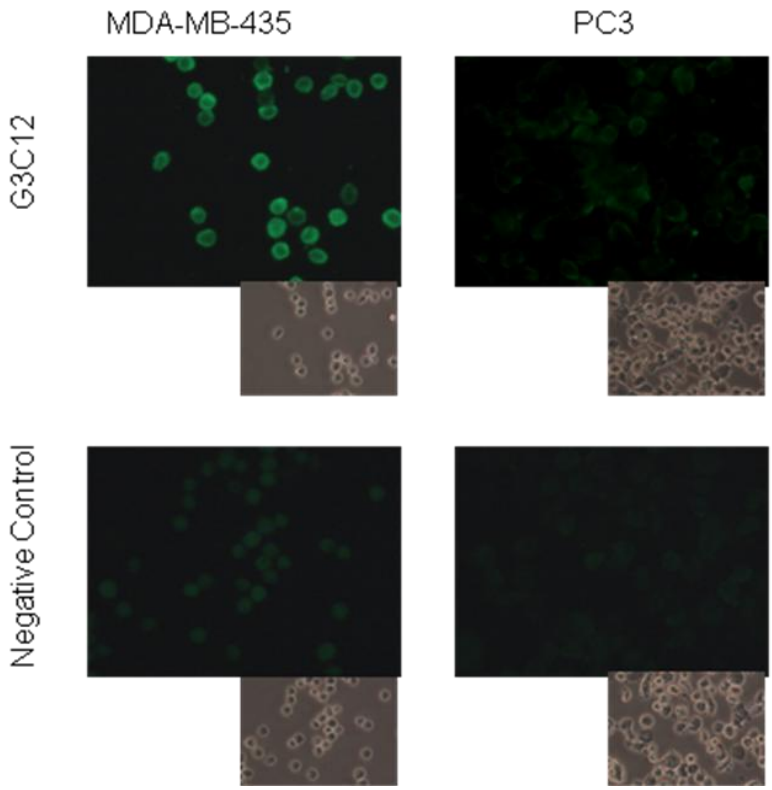

Fig. 7. Binding of peptides to gal-3 displayed on cultured human tissue cells, MDA-MB-435 human breast cancer cells (positive for gal-3) and PC-3 prostate cancer cells (negative for gal-3). Peptides used include G3-C12 test peptide, and scrambled point mutation peptide as negative control. Binding was detected with Oregon Green (10 μg/ml) and confocal microscopy.

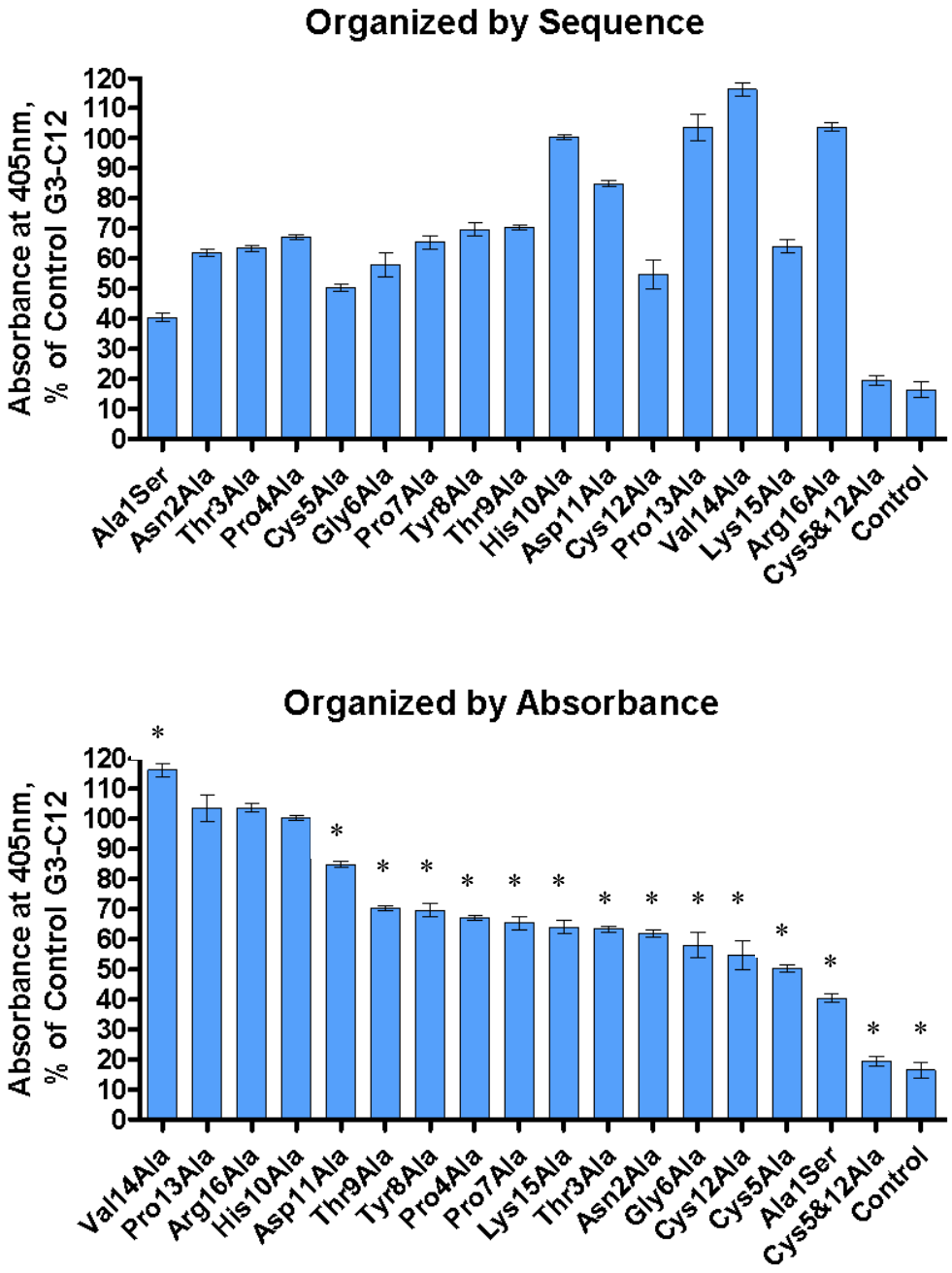

Fig. 8. Gal-3 peptides binding to immobilized gal-3 using ELISA experiments. Binding potential of mutant peptides was determined by interaction of biotinylated peptides in solution (1µM) with immobilized gal -3 (0.5 ug). Colorimetric detection with use of Streptavidin-HRP as secondary and ,2'-Azino-Bis (3-ethylbenzthiazoline-6-Sulfonic Acid) as developer. Wells with no gal-3 were used as blanks. Percent binding was calculated as the percentage of absorbance at 405 nm compared to absorbance of G3-C12 peptide. A T-test was performed on the data and a * on the organized by absorbance graph indicates a p-value of less than 0.05, indicating statistical significance.

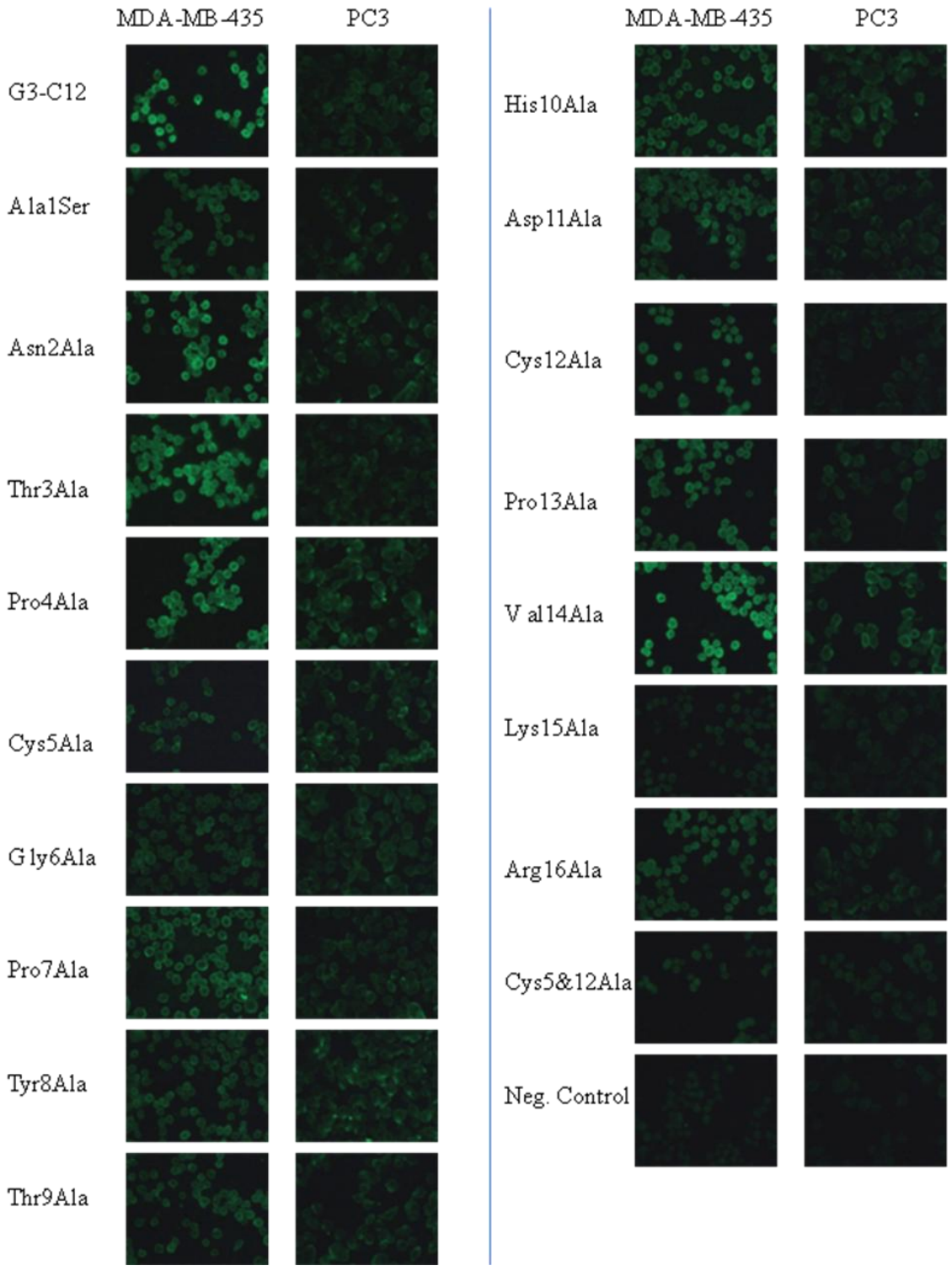

Fig. 9. Binding of biotinylated point mutation peptides to gal-3 displayed on cultured human tissue cells, MDA-MB-435 human breast cancer cells (positive for gal-3) and PC-3 prostate cancer cells (negative for gal-3) Laser confocal scanning microscopic examination of cell-surface binding of peptides (20 μM) was done with detection using Oregon Green (10 μg/ml).

A

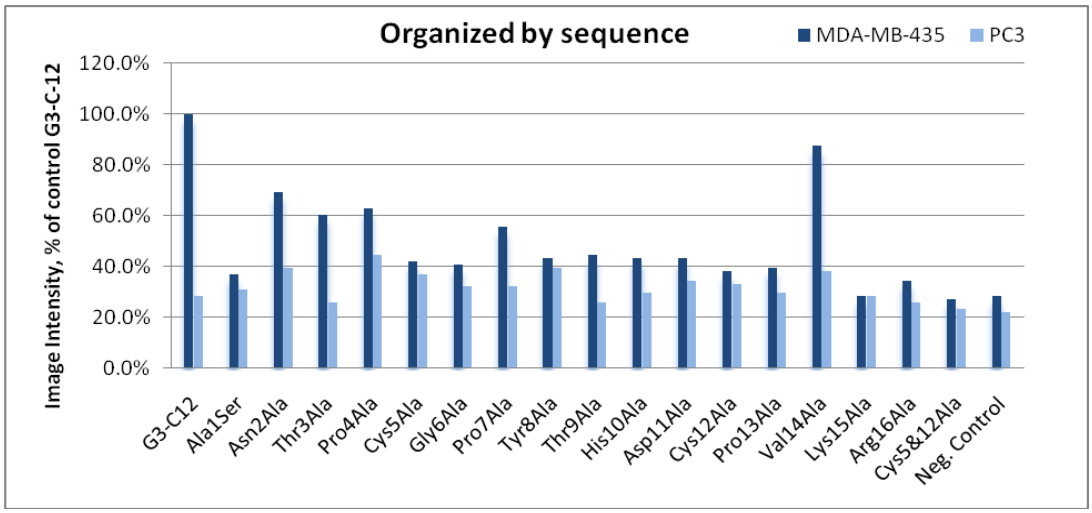

B

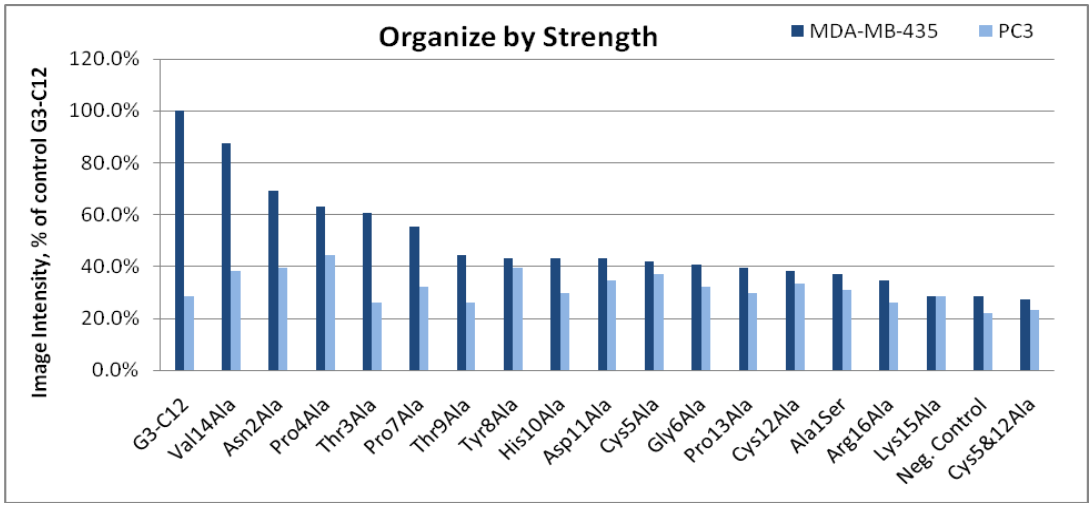

Fig. 10. Intensity of binding of biotinylated point mutation peptides to gal-3 displayed on cultured human tissue cells, MDA-MB-435 human breast cancer cells (positive for gal-3) and PC-3 prostate cancer cells (negative for gal-3) Image J software was used to quantify the intensity of the signal in figure 9. (A) Mutations presented in sequence order (B) Mutations presented in signal strength order.

CHAPTER 4- SUMMARY

The purpose of this study was to take a novel biomarker targeting peptide and develop it into potential diagnostic cancer imaging agents and increase understanding of key residues of another novel biomarker targeting peptide. $^{99m}Tc(CO)_3$-DAP-GSG-KCCYSL and $^{99m}Tc(CO)_3$-(NαHis)Ac-GSG-KCCYSL were evaluated for their biodistribution and SPECT/CT imaging in SCID female mice bearing MDA-MB-435 human breast carcinomas. Selective tumor uptake in the tumor and rapid clearance from nontarget organs underscores the potential both peptide constructs have as radiolabeled agents for the detection of ErbB-2 positive human breast carcinoma. Improved hydrophilicity of the $^{99m}Tc(CO)_3$ complexes will reduce nonspecific hydrophobic interactions enhancing tumor to normal tissue ratios resulting in greater imaging sensitivity, and thus greater ability for use as diagnostic scans for breast cancer.

An increase in the understanding of key residues in a phage display selected targeting peptide is the first step in the creation of a radiolabeled imaging agent. Through several methods, the key residues in the G3-C12 peptide were determined to be the Ala in position 1 and the Cys in position 5 and 12, with particular focus on residues 5 and 12 together. This focuses attention to the potential interaction between disulfide bridges and the interaction between gal-3 protein and G3-C12 peptide. More experiments to study binding mechanism and radiolabeling will bring peptide G3-C12 toward development as another potential diagnostic cancer imaging agent. The development of better diagnostic cancer imaging agents will lead to earlier diagnosis of cancer, and a reduction on the number of severe and life threatening cases of cancer.

REFERENCES

1. *Cancer Facts and Figures.*
2. Williams-Brown, S. and G.K. Singh, *Epidemiology of cancer in the United States.* Semin Oncol Nurs, 2005. **21**(4): p. 236-42.
3. Hinestrosa, M.C., et al., *Shaping the future of biomarker research in breast cancer to ensure clinical relevance.* Nat Rev Cancer, 2007. **7**(4): p. 309-15.
4. Landgraf, R., *HER2 therapy. HER2 (ERBB2): functional diversity from structurally conserved building blocks.* Breast Cancer Res, 2007. **9**(1): p. 202.
5. Koutsopoulos, A.V., et al., *Simultaneous expression of c-erbB-1, c-erbB-2, c-erbB-3 and c-erbB-4 receptors in non-small-cell lung carcinomas: correlation with clinical outcome.* Lung Cancer, 2007. **57**(2): p. 193-200.
6. Hynes, N.E. and D.F. Stern, *The biology of erbB-2/neu/HER-2 and its role in cancer.* Biochimica et Biophysica Acta, 1994. **1198**: p. 165-84.
7. Arpino, G., et al., *Treatment of human epidermal growth factor receptor 2-overexpressing breast cancer xenografts with multiagent HER-targeted therapy.* J Natl Cancer Inst, 2007. **99**(9): p. 694-705.
8. Murphy, A.J., et al., *Low-level TOP2A amplification in prostate cancer is associated with HER2 duplication, androgen resistance, and decreased survival.* Cancer Res, 2007. **67**(6): p. 2893-8.
9. Tan, M., J. Yao, and D. Yu, *Overexpression of the c-erbB-2 gene enhanced intrinsic metastasis potential in human breast cancer cells without increasing their transformation abilities.* Cancer Res, 1997. **57**(6): p. 1199-205.
10. Yang, S., et al., *Mapping ErbB receptors on breast cancer cell membranes during signal transduction.* J Cell Sci, 2007. **120**(Pt 16): p. 2763-73.
11. Nagy, P., et al., *Activation-dependent clustering of the erbB2 receptor tyrosine kinase detected by scanning near-field optical microscopy.* J Cell Sci, 1999. **112 (Pt 11)**: p. 1733-41.
12. Felip, E., et al., *Overexpression of e-erbB-2 in epithelial ovarian cancer. Prognostic value and relationships with response to chemotherapy.* Cancer, 2006. **75**: p. 2147-2152.
13. Mayr, D., et al., *HER-2/neu gene amplification in ovarian tumours: a comprehensive immunohistochemical and FISH analysis on tissue microarrays.* Histopathology, 2006. **48**(2): p. 149-56.
14. Raz, A. and R. Lotan, *Endogenous galactoside-binding lectins: a new class of functional tumor cell surface molecules related to metastasis.* Cancer & Metastasis Reviews, 1987. **6**: p. 433-52.
15. Le Marer, N. and R.C. Hughes, *Effects of the carbohydrate-binding protein galectin-3 on the invasiveness of human breast carcinoma cells.* J Cell Physiol, 1996. **168**: p. 51-8.
16. Nangia-Makker, P., et al., *Galectin-3 induces endothelial cell morphogenesis and angiogenesis.* American Journal of Pathology, 2000. **156**: p. 899-909.
17. Springer, G.F., *T and Tn, general carcinoma autoantigens.* Science, 1984. **224**(4654): p. 1198-206.

18. Glinsky, V.V., et al., *The role of Thomsen-Friedenreich antigen in adhesion of human breast and prostate cancer cells to the endothelium.* Cancer Research, 2001. **61**: p. 4851-7.
19. Glinsky, V.V., et al., *Effects of Thomsen-Friedenreich antigen-specific peptide P-30 on beta-galactoside-mediated homotypic aggregation and adhesion to the endothelium of MDA-MB-435 human breast carcinoma cells.* Cancer Research, 2000. **60**: p. 2584-8.
20. Glinsky, V.V., et al., *Intravascular metastatic cancer cell homotypic aggregation at the sites of primary attachment to the endothelium.* Cancer Research, 2003. **63**: p. 3805-11.
21. Khaldoyanidi, S.K., et al., *MDA-MB-435 human breast carcinoma cell homo- and heterotypic adhesion under flow conditions is mediated in part by Thomsen-Friedenreich antigen-galectin-3 interactions.* Journal of Biological Chemistry, 2003. **278**: p. 4127-34.
22. Parmley, S.F. and G.P. Smith, *Antibody-selectable filamentous fd phage vectors: affinity purification of target genes.* Gene, 1988. **73**: p. 305-18.
23. Smith, G.P., *Filamentous fusion phage: novel expression vectors that display cloned antigens on the virion surface.* Science, 1985. **228**(4705): p. 1315-7.
24. Goldenberg, M.M., *Trastuzumab, a recombinant DNA-derived humanized monoclonal antibody, a novel agent for the treatment of metastatic breast cancer.* Clin Ther, 1999. **21**(2): p. 309-18.
25. Lub-de Hooge, M.N., et al., *Preclinical characterisation of 111In-DTPA-trastuzumab.* British Journal of Pharmacology, 2004. **143**: p. 99-106.
26. Deshpande, S.V., et al., *Yttrium-90-labeled monoclonal antibody for therapy: labeling by a new macrocyclic bifunctional chelating agent.* J Nucl Med, 1990. **31**(4): p. 473-9.
27. Klastersky, J., *Adverse effects of the humanized antibodies used as cancer therapeutics.* Curr Opin Oncol, 2006. **18**(4): p. 316-20.
28. Okarvi, S.M., *Recent developments in 99Tcm-labelled peptide-based radiopharmaceuticals: an overview.* Nuclear Medicine Communications, 1999. **20**: p. 1093-112.
29. Blok, D., et al., *Peptide radiopharmaceuticals in nuclear medicine.* European Journal of Nuclear Medicine, 1999. **26**: p. 1511-9.
30. Boerman, O.C., W.J. Oyen, and F.H. Corstens, *Radio-labeled receptor-binding peptides: a new class of radiopharmaceuticals.* Seminars in Nuclear Medicine, 2000. **30**: p. 195-208.
31. Fischman, A.J., J.W. Babich, and H.W. Strauss, *A ticket to ride: peptide radiopharmaceuticals.* J Nucl Med, 1993. **34**(12): p. 2253-63.
32. Weiner, L.M., et al., *Phase I trial of 2B1, a bispecific monoclonal antibody targeting c-erbB-2 and Fc gamma RIII.* Cancer Res, 1995. **55**(20): p. 4586-93.
33. Jinno, H., et al., *Effectiveness of an adriamycin immunoconjugate that recognizes the C-erbB-2 product on breast cancer cell lines.* Surg Today, 1996. **26**(7): p. 501-7.
34. Disis, M.L., et al., *Generation of immunity to the HER-2/neu oncogenic protein in patients with breast and ovarian cancer using a peptide-based vaccine.* Clin Cancer Res, 1999. **5**(6): p. 1289-97.

35. Harris, J.D., et al., *Gene therapy for cancer using tumour-specific prodrug activation.* Gene Ther, 1994. **1**(3): p. 170-5.
36. Baselga, J., et al., *Recombinant humanized anti-HER2 antibody (Herceptin) enhances the antitumor activity of paclitaxel and doxorubicin against HER2/neu overexpressing human breast cancer xenografts.* Cancer Res, 1998. **58**(13): p. 2825-31.
37. Cobleigh, M.A., et al., *Multinational study of the efficacy and safety of humanized anti-HER2 monoclonal antibody in women who have HER2-overexpressing metastatic breast cancer that has progressed after chemotherapy for metastatic disease.* J Clin Oncol, 1999. **17**(9): p. 2639-48.
38. Karasseva, N., et al., *Identification and characterization of peptides that bind human ErbB-2 selected from a bacteriophage display library.* Journal of Protein Chemistry, 2002. **21**: p. 287-296.
39. Kumar, S.R., T.P. Quinn, and S.L. Deutscher, *Evaluation of an 111In-radiolabeled peptide as a targeting and imaging agent for ErbB-2 receptor expressing breast carcinomas.* Clin Cancer Res, 2007. **13**(20): p. 6070-9.
40. Landon, L.A., et al., *Combinatorial evolution of high affinity peptides that bind to the Thomsen-Friedenreich carcinoma antigen.* Journal of Protein Chemistry, 2003. **22**: p. 193-204.
41. Landon, L.A., et al., *High throughput fluorescence spectroscopic analysis of binding affinity of peptides displayed on bacteriophage.* Analytical Biochemistry, 2004. **331**: p. 60-67.
42. Landon, L.A., J. Zou, and S.L. Deutscher, *An Effective Combinatorial Strategy to Increase Affinity of Carbohydrate Binding by Peptides.* Molecular Diversity, 2003. **8**: p. 35-50.
43. Kumar, S.R. and S.L. Deutscher, *111In-labeled galectin-3-targeting peptide as a SPECT agent for imaging breast tumors.* J Nucl Med, 2008. **49**(5): p. 796-803.
44. Zou, J., et al., *Peptides specific to the galectin-3 carbohydrate recognition domain inhibit metastasis-associated cancer cell adhesion.* Carcinogenesis, 2005. **26**: p. 309-318.
45. Kennel, S.J., et al., *Labeling and distribution of linear peptides identified using in vivo phage display selection for tumors.* Nuclear Medicine and Biology, 2000. **27**: p. 815-25.
46. Anderson, C.J. and M.J. Welch, *Radiometal-labeled agents (non-technitium) for diagnostic imaging.* Chemical Reviews, 1999. **99**: p. 2219-2234.
47. Bakker, W.H., et al., *In vivo application of [111In-DTPA-D-Phe1]-octreotide for detection of somatostatin receptor-positive tumors in rats.* Life Sciences, 1991. **49**: p. 1593-601.
48. Krenning, E.P., et al., *Somatostatin receptor scintigraphy with indium-111-DTPA-D-Phe-1-octreotide in man: metabolism, dosimetry and comparison with iodine-123-Tyr-3-octreotide.* J Nucl Med, 1992. **33**(5): p. 652-8.
49. Thakur, M.L., et al., *Indium-LLL labeled platelets: studies on preparation and evaluation of in vitro and in vivo functions.* Thromb Res, 1976. **9**(4): p. 345-57.
50. Bourguignon, M.H., G. Loc'h, and B. Maziere, *The future of SPECT radioisotopes: technetium-99m or iodine-123?* Journal of Nuclear Biology and Medicine, 1994. **38**: p. 573-5.

51. Jurisson, S.S. and J.D. Lydon, *Potential technetium small molecule radiopharmaceuticals.* Chem Rev, 1999. **99**(9): p. 2205-18.
52. Jurisson, S., et al., *Coordination Compounds in Nuclear Medicine.* Chemical Reviews, 1993. **93**(3): p. 1137-1156.
53. Fornell, D., *SPECT vs PET, Which is Best?* Diagnostic and Invasive Cardiology, 2008.
54. Chen, J., et al., *Alpha-melanocyte-stimulating hormone peptide analogs labeled with technetium-99m and indium-111 for malignant melanoma targeting.* Cancer, 2002. **94**: p. 1196-201.
55. Chen, J., et al., *Melanoma-targeting properties of (99m)technetium-labeled cyclic alpha-melanocyte-stimulating hormone peptide analogues.* Cancer Res, 2000. **60**(20): p. 5649-58.
56. Chen, J., et al., *Evaluation of an (111)In-DOTA-rhenium cyclized alpha-MSH analog: a novel cyclic-peptide analog with improved tumor-targeting properties.* Journal of Nuclear Medicine, 2001. **42**: p. 1847-55.
57. Cheng, Z., et al., *Modification of the structure of a metallopeptide: synthesis and biological evaluation of (111)In-labeled DOTA-conjugated rhenium-cyclized alpha-MSH analogues.[erratum appears in J Med Chem 2002 Sep 26;45(20):4588].* Journal of Medicinal Chemistry, 2002. **45**: p. 3048-56.
58. Miao, Y., K. Benwell, and T.P. Quinn, *99mTc- and 111In-labeled alpha-melanocyte-stimulating hormone peptides as imaging probes for primary and pulmonary metastatic melanoma detection.* J Nucl Med, 2007. **48**(1): p. 73-80.
59. Hnatowich, D.J., et al., *Labeling Peptides with Technetium-99m using a Bifunctional Chelator of a N-Hydroxysuccinimide Ester of Mercaptoacetyltriglycine.* Journal of Nuclear Medicine, 1998. **39**(1): p. 56-64.
60. Smith, C.J., et al., *Radiochemical investigations of [188Re(H2O)(CO)3-diaminopropionic acid-SSS-bombesin(7-14)NH2]: syntheses, radiolabeling and in vitro/in vivo GRP receptor targeting studies.* Anticancer Res, 2003. **23**(1A): p. 63-70.
61. Schibli, R., et al., *Influence of the denticity of ligand systems on the in vitro and in vivo behavior of (99m)Tc(I)-tricarbonyl complexes: a hint for the future functionalization of biomolecules.* Bioconjugate Chemistry, 2000. **11**: p. 345-51.
62. La Bella, R., et al., *In vitro and in vivo evaluation of a 99mTc(I)-labeled bombesin analogue for imaging of gastrin releasing peptide receptor-positive tumors.* Nucl Med Biol, 2002. **29**(5): p. 553-60.
63. Alberto, R., et al., *A Novel Organometallic Aqua Complex of Technetium for the Labeling of Biomolecules: Synthesis of [99mTc(OH2)3(CO)3]+ from [99mTcO4]- in Aqueous Solution and Its Reaction with a Bifunctional Ligand.* Journal of the American Chemical Society, 1998. **120**(31): p. 7987-7988.
64. Alberto, R., et al., *Basic aqueous chemistry of [M(OH2)3(CO)3]+ (M=Re, Tc) directed towards radiopharmaceutical application.* Coordination Chemistry Reviews, 1999. **190-192**: p. 901-919.
65. Smith, C.J., et al., *Radiochemical investigations of gastrin-releasing peptide receptor-specific [(99m)Tc(X)(CO)3-Dpr-Ser-Ser-Ser-Gln-Trp-Ala-Val-Gly-His-Leu-Met-(NH2)] in PC-3, tumor-bearing, rodent models: syntheses, radiolabeling,*

and in vitro/in vivo studies where Dpr = 2,3-diaminopropionic acid and X = H2O or P(CH2OH)3. Cancer Research, 2003. **63**: p. 4082-8.
66. Garcia Garayoa, E., et al., *Chemical and biological characterization of new Re(CO)3/[99mTc](CO)3 bombesin analogues.* Nucl Med Biol, 2007. **34**(1): p. 17-28.
67. Prasanphanich, A.F., et al., *The effects of linking substituents on the in vivo behavior of site-directed, peptide-based, diagnostic radiopharmaceuticals.* In Vivo, 2007. **21**(1): p. 1-16.
68. Bagossi, P., et al., *Molecular modeling of nearly full-length ErbB2 receptor.* Biophys J, 2005. **88**(2): p. 1354-63.
69. Altomare, D.A., et al., *AKT and mTOR phosphorylation is frequently detected in ovarian cancer and can be targeted to disrupt ovarian tumor cell growth.* Oncogene, 2004. **23**(34): p. 5853-7.
70. Xia, W., et al., *Anti-tumor activity of GW572016: a dual tyrosine kinase inhibitor blocks EGF activation of EGFR/erbB2 and downstream Erk1/2 and AKT pathways.* Oncogene, 2002. **21**(41): p. 6255-63.
71. Saez, R., et al., *p95HER-2 predicts worse outcome in patients with HER-2-positive breast cancer.* Clin Cancer Res, 2006. **12**(2): p. 424-31.
72. Tolmachev, V., et al., *Radionuclide therapy of HER2-positive microxenografts using a 177Lu-labeled HER2-specific Affibody molecule.* Cancer Res, 2007. **67**(6): p. 2773-82.
73. Jackson, J.G., et al., *Blockade of epidermal growth factor- or heregulin-dependent ErbB2 activation with the anti-ErbB2 monoclonal antibody 2C4 has divergent downstream signaling and growth effects.* Cancer Res, 2004. **64**(7): p. 2601-9.
74. Johnson, B.E. and P.A. Janne, *Rationale for a phase II trial of pertuzumab, a HER-2 dimerization inhibitor, in patients with non-small cell lung cancer.* Clin Cancer Res, 2006. **12**(14 Pt 2): p. 4436s-4440s.
75. Reubi, J.C., *Peptide receptors as molecular targets for cancer diagnosis and therapy.* Endocr Rev, 2003. **24**(4): p. 389-427.
76. Bakker, W.H., et al., *In vivo application of [111In-DTPA-D-Phe1]-octreotide for detection of somatostatin receptor-positive tumors in rats.* Life Sci, 1991. **49**(22): p. 1593-601.
77. Gotthardt, M., et al., *Indication for different mechanisms of kidney uptake of radiolabeled peptides.* J Nucl Med, 2007. **48**(4): p. 596-601.
78. Akizawa, H., T. Uehara, and Y. Arano, *Renal uptake and metabolism of radiopharmaceuticals derived from peptides and proteins.* Adv Drug Deliv Rev, 2008. **60**(12): p. 1319-28.
79. Tsai, S.W., et al., *Metabolism and renal clearance of 111In-labeled DOTA-conjugated antibody fragments.* Bioconjug Chem, 2001. **12**(2): p. 264-70.
80. Rogers, B.E., et al., *Identification of metabolites of 111In-diethylenetriaminepentaacetic acid-monoclonal antibodies and antibody fragments in vivo.* Cancer Res, 1995. **55**(23 Suppl): p. 5714s-5720s.
81. Miao, Y., et al., *In vivo evaluation of 188Re-labeled alpha-melanocyte stimulating hormone peptide analogs for melanoma therapy.* International Journal of Cancer, 2002. **101**: p. 480-7.

82. Behr, T.M., et al., *Reduction of the renal uptake of radiolabeled monoclonal antibody fragments by cationic amino acids and their derivatives.* Cancer Res, 1995. **55**(17): p. 3825-34.
83. Behr, T.M., D.M. Goldenberg, and W. Becker, *Reducing the renal uptake of radiolabeled antibody fragments and peptides for diagnosis and therapy: present status, future prospects and limitations.* Eur J Nucl Med, 1998. **25**(2): p. 201-12.
84. Silbernagl, S., *The renal handling of amino acids and oligopeptides.* Physiol Rev, 1988. **68**(3): p. 911-1007.
85. Rolleman, E.J., et al., *Uptake of [111In-DTPA0]octreotide in the rat kidney is inhibited by colchicine and not by fructose.* J Nucl Med, 2004. **45**(4): p. 709-13.
86. de Jong, M., et al., *Megalin is essential for renal proximal tubule reabsorption of (111)In-DTPA-octreotide.* J Nucl Med, 2005. **46**(10): p. 1696-700.
87. Miao, Y., D.R. Fisher, and T.P. Quinn, *Reducing renal uptake of 90Y- and 177Lu-labeled alpha-melanocyte stimulating hormone peptide analogues.* Nucl Med Biol, 2006. **33**(6): p. 723-33.
88. van Eerd, J.E., et al., *Gelatin-based plasma expander effectively reduces renal uptake of 111In-octreotide in mice and rats.* J Nucl Med, 2006. **47**(3): p. 528-33.
89. Rolleman, E.J., et al., *Molecular imaging of reduced renal uptake of radiolabelled [DOTA0,Tyr3]octreotate by the combination of lysine and Gelofusine in rats.* Nuklearmedizin, 2008. **47**(3): p. 110-5.
90. Vegt, E., et al., *Renal uptake of radiolabeled octreotide in human subjects is efficiently inhibited by succinylated gelatin.* J Nucl Med, 2006. **47**(3): p. 432-6.
91. Vegt, E., et al., *Reducing renal uptake of radiolabeled peptides using albumin fragments.* J Nucl Med, 2008. **49**(9): p. 1506-11.
92. Rolleman, E.J., et al., *Safe and effective inhibition of renal uptake of radiolabelled octreotide by a combination of lysine and arginine.* Eur J Nucl Med Mol Imaging, 2003. **30**(1): p. 9-15.
93. Raposinho, P.D., et al., *A (99m)Tc(CO)(3)-labeled pyrazolyl-alpha-melanocyte-stimulating hormone analog conjugate for melanoma targeting.* Nucl Med Biol, 2008. **35**(1): p. 91-9.
94. Alves, S., et al., *In vitro and in vivo evaluation of a novel 99mTc(CO)3-pyrazolyl conjugate of cyclo-(Arg-Gly-Asp-d-Tyr-Lys).* Bioconjug Chem, 2007. **18**(2): p. 530-7.
95. Sharkey, R.M. and D.M. Goldenberg, *Perspectives on cancer therapy with radiolabeled monoclonal antibodies.* J Nucl Med, 2005. **46 Suppl 1**: p. 115S-27S.
96. Ward, E.S., et al., *Binding activities of a repertoire of single immunoglobulin variable domains secreted from Escherichia coli.[comment].* Nature, 1989. **341**: p. 544-6.
97. Behr, T.M., et al., *Imaging tumors with peptide-based radioligands.* Q J Nucl Med, 2001. **45**(2): p. 189-200.
98. Orr, F.W., et al., *Interactions between cancer cells and the endothelium in metastasis.* J Pathol, 2000. **190**: p. 310-29.
99. Springer, G.F., P.R. Desai, and I. Banatwala, *Blood group MN antigens and precursors in normal and malignant human breast glandular tissue.* Journal of the National Cancer Institute, 1975. **54**: p. 335-9.

100. Andre, S., et al., *Galectins-1 and -3 and their ligands in tumor biology. Non-uniform properties in cell-surface presentation and modulation of adhesion to matrix glycoproteins for various tumor cell lines, in biodistribution of free and liposome-bound galectins and in their expression by breast and colorectal carcinomas with/without metastatic propensity.* Journal of Cancer Research & Clinical Oncology., 1999. **125**: p. 461-74.